Velocity, Turbulence, and Sediment Deposition in a Channel Partially Filled With a Phragmites australis Canopy

AGU ADVANCING EARTH AND SPACE SCIENCE

Water Resources Research

RESEARCH ARTICLE
10.1029/2022WR032381

Velocity, Turbulence, and Sediment Deposition in a Channel Partially Filled With a *Phragmites australis* Canopy

Chao Liu[1], Chunhao Yan[1,2], Sichen Sun[1], Jiarui Lei[3], Heidi Nepf[4], and Yuqi Shan[1,5]

[1]State Key Laboratory of Hydraulics and Mountain River Engineering, Sichuan University, Chengdu, China, [2]Chongqing Southwest Research Institute for Water Transport Engineering, Chongqing Jiaotong University, Chongqing, China, [3]Civil and Environmental Engineering, National University of Singapore, Singapore, Singapore, [4]Department of Civil and Environmental Engineering, Massachusetts Institute of Technology, Cambridge, MA, USA, [5]Institute for Disaster Management and Reconstruction, Sichuan University, Chengdu, China

Key Points:

- Methods for predicting the evolution of near-bed velocity, TKE, and net deposition inside a *Phragmites australis* canopy were proposed and validated
- Net deposition in the canopy was enhanced only when TKE was below a critical value and resuspension took place in the bare channel
- The proposed model can predict the critical solid volume fraction for enhanced in-canopy deposition relative to deposition for bare beds

Supporting Information:

Supporting Information may be found in the online version of this article.

Correspondence to:

Y. Shan,
yuqi_shan@qq.com

Citation:

Liu, C., Yan, C., Sun, S., Lei, J., Nepf, H., & Shan, Y. (2022). Velocity, turbulence, and sediment deposition in a channel partially filled with a *Phragmites australis* canopy. *Water Resources Research*, *58*, e2022WR032381. https://doi.org/10.1029/2022WR032381

Received 15 MAR 2022
Accepted 22 JUL 2022

Author Contributions:

Conceptualization: Chao Liu
Formal analysis: Chunhao Yan
Funding acquisition: Chao Liu, Yuqi Shan
Investigation: Chunhao Yan, Sichen Sun
Methodology: Chao Liu
Project Administration: Chao Liu
Supervision: Chao Liu, Heidi Nepf, Yuqi Shan
Validation: Chao Liu, Yuqi Shan
Writing – original draft: Chao Liu
Writing – review & editing: Chao Liu, Jiarui Lei, Heidi Nepf, Yuqi Shan

Abstract Laboratory experiments examined the longitudinal evolution of near-bed velocity, turbulent kinetic energy (TKE), and net deposition in a model *Phragmites australis* canopy occupying 1/3 of the channel width. The canopies were constructed from model *P. australis* with real morphology and a solid volume fraction between 0.003 and 0.018. An exponential model was modified to predict the longitudinal evolution of near-bed velocity inside the canopy, from which the near-bed TKE can be predicted. By combining the predicted TKE and a deposition probability, we proposed a model to predict the distribution of net deposition inside the canopy. The predicted velocity, TKE, and deposition were in good agreement with the measurements. Relative to an upstream reference, the net deposition within the canopy was enhanced when two conditions were met: the in-canopy, near-bed TKE was smaller than the critical value for resuspension, and resuspension took place in the bare channel. Above a critical vegetation density (defined by a critical solid volume fraction ϕ_c), the spatially-averaged deposition inside *P. australis* surpassed that in the adjacent bare channel. The proposed model provides a way to estimate ϕ_c. Relative to the upstream reference, deposition inside the canopy was always diminished over some fraction of the flow adjustment distance, L_d (distance from canopy leading edge to fully developed flow). When the canopy length was greater than 0.4 L_d, canopy-averaged deposition was enhanced relative to the bare channel. Finally, for the same canopy length, differences in plant morphologies did not have a strong impact on the in-canopy deposition distribution.

1. Introduction

Aquatic vegetation is widely observed in rivers, streams, marshes, and coastal regions and influences these ecosystems by altering flow structure and modifying bed morphology (Bouma et al., 2007; Elliott et al., 2019; Gu et al., 2019; Huai et al., 2019; Li et al., 2021; Licci et al., 2019; Liu et al., 2016; Manners et al., 2015; Nepf, 2012; Sand-Jensen & Pedersen, 2008; Shan et al., 2017; Vandenbruwaene et al., 2011; Widdows et al., 2008). Vegetation provides drag that shapes the spatial distribution of velocity and turbulent kinetic energy (TKE) and impacts sediment transport and bedforms within vegetated regions (e.g., Gu et al., 2019; Kim et al., 2015; Zong & Nepf, 2011). Specifically, compared to a bare channel, velocity in a vegetated region is reduced due to vegetation drag, and diminished velocity promotes sediment retention (e.g., Cotton et al., 2006; Huai et al., 2021; Liu et al., 2020). Meanwhile, in vegetated regions, vegetation-generated turbulence enhances TKE, which can promote sediment resuspension (e.g., Liu et al., 2021; Tinoco & Coco, 2016; Zong & Nepf, 2010, 2011). These competing trends (sediment retention vs. resuspension) exist simultaneously and make it difficult to predict the balance of deposition and erosion that dictates the evolution of vegetated landscapes. Given the significance of vegetation in shaping landscapes, it is important to understand how current interacts with vegetation and, in particular, affects the velocity, TKE, and sediment deposition inside canopies.

In this study, we considered an emergent canopy of model *Phragmites australis* distributed along the sidewall of a channel. By considering the real morphology of *P. australis*, which varies with distance from the bed, this study advances our understanding beyond the many previous studies that considered arrays of circular cylinders to represent vegetation patches (e.g., Liu & Shan, 2019, 2022; Liu et al., 2020; Rominger & Nepf, 2011; White & Nepf, 2008). Because cylinders have vertically uniform frontal area, flow adjustment at the leading edge of an emergent cylinder array only occurs in the horizontal plane, resulting in diminished velocity inside the patch and enhanced velocity in the adjacent bare channel (e.g., Liu et al., 2020; White & Nepf, 2008). The distance within

the array over which the time-averaged velocity decreases to its fully developed distribution is defined by the interior flow adjustment distance, L_d. For a rigid cylinder array located at mid-channel, Rominger and Nepf (2011) showed that L_d was related to the frontal area per canopy volume, a (defined using the solid plus fluid volume), the canopy drag coefficient, C_d, and the patch half-width, b:

$$L_d = (5.5 \pm 0.4)\sqrt{\left(\frac{2}{C_d a}\right)^2 + b^2} \qquad \text{for } C_d ab \geq 1 \tag{1a}$$

$$L_d = (3.0 \pm 0.3)\left[\frac{2}{C_d a}\left(1 + (C_d ab)^2\right)\right] \text{ for } C_d ab < 1 \tag{1b}$$

For an array situated at the wall, as in this study, the wall can be regarded as a line of symmetry, such that b is equivalent to the full patch-width. In the present study, the frontal area of *P. australis* varied with distance from the bed (z), that is, $a = f(z)$; thus, we examined whether Equation 1 could be applied to this more realistic canopy using the depth-averaged (subscript "d") frontal area, $a_d\left(= \frac{1}{H}\int_0^H a(z)dz\right)$, in which H is the flow depth.

For an emergent canopy, for $x > L_d$, Kelvin-Helmholtz (KH) vortices form along the side edge of the canopy if the shear strength is sufficient. Specifically, for a canopy located at the wall of a channel, KH vortices form if canopy drag exceeds the wall drag, defined by $ab > 0.1$, based on scale analysis, but may be suppressed if bed friction is sufficient (White & Nepf, 2007). Similarly, Caroppi et al. (2020) found that KH vortices occurred only when the lateral shear was sufficient, defined by the shear parameter $\lambda\left(= \frac{U_{bare} - U_{veg}}{U_{bare} + U_{veg}}\right) \geq 0.4$, in which U_{bare} and U_{veg} are the mean velocity of the bare channel and vegetated region, respectively. When KH vortices form, they penetrate through the side edge into the patch over a penetration distance, δ_p. For an emergent cylinder array, White and Nepf (2008) suggested that the penetration distance can be estimated $\delta_p = \max[0.5(C_d a)^{-1}, 1.8d]$, in which d is the cylinder diameter. For common aquatic plants, the frontal area per canopy volume is $a = 0.01$–$0.13\ \text{cm}^{-1}$, and the stem diameter is $d = 0.2$–1.2 cm (Lightbody & Nepf, 2006; Widdows et al., 2008), so that a typical penetration distance is $\delta_p = 4$–50 cm, assuming $C_d = 1$. In many natural conditions, the canopy width, b, is on the order of meters to 10 m (e.g., Cornacchia et al., 2018; Cotton et al., 2006; Widdows et al., 2008), such that $\delta_p/b << 1$. Farther inside the canopy, $b - \delta_p > y \geq 0$ with the channel side wall at $y = 0$, the spatial-average velocity is not influenced by the momentum flux contributed by the KH vortices. Since many canopies exhibit $\delta_p/b << 1$, it is reasonable to focus on the interior region of the canopy ($b - \delta_p > y \geq 0$), which is the approach taken in the present study.

Within an emergent canopy, velocity decreases from the leading edge ($x = 0$), which can be represented by an exponential decay (e.g., Belcher et al., 2003; Chen et al., 2013). Modifying Chen et al. (2013), Liu et al. (2020) described and validated the following model for the longitudinal evolution of velocity, U, in the interior region ($y < b - \delta_p$) of an emergent canopy of uniform frontal area:

$$U = U_{(f)} + (U_{(0)} - U_{(f)})\, e^{-\frac{3x}{L_d}} \tag{2}$$

in which $U_{(f)}$ is the velocity in the fully developed flow region of the canopy ($x > L_d$) and $U_{(0)}$ is the velocity at the leading edge of the canopy ($x = 0$).

Based on the steady momentum balance, the velocity in the fully developed flow region within an emergent canopy is:

$$U_{(f)} = \sqrt{\frac{gHS}{C_f + \frac{C_d a H}{2(1-\phi)}}} \tag{3}$$

in which g is the gravitational acceleration, S is the water surface and/or bed slope, C_f is the bed friction coefficient, and ϕ is the solid volume fraction of the canopy. For cylinders, $a = nd$, with n the cylinders per bed area. Equations 2 and 3 were developed for a cylinder array with uniform frontal area, for which the velocity is essentially uniform over depth. The present study considered the extension to natural canopies with a non-uniform

frontal area, specifically a model of *P. australis* (Figure 1). The velocity model was used to predict the evolution of near-bed TKE along the canopy.

Previous studies have investigated sediment resuspension and deposition within vegetation modeled by arrays of circular stems (e.g., Liu et al., 2021; Shi et al., 2016; Tinoco & Coco, 2016; Tseng & Tinoco, 2021; Zong & Nepf, 2010). For emergent arrays, the stem density and mean channel velocity determine the velocity and turbulence within the canopy, which in turn impacts resuspension and deposition (e.g., Zong & Nepf, 2011). Diminished or enhanced deposition within the canopy, relative to the adjacent bare bed, has been linked to the presence or absence of vegetation-generated turbulence, respectively (Liu & Nepf, 2016). For example, Zong and Nepf (2010) measured net deposition within an emergent array of circular stems constructed along a channel sidewall. Although they observed diminished velocity and bed shear stress within the leading edge of the array, reduced deposition was reported in this region relative to the upstream bare channel, which was attributed to elevated turbulence intensity associated with stem-generated turbulence. Inside the array, they observed enhanced deposition relative to the bare bed, which was associated with diminished turbulence beyond the interior flow adjustment distance, L_d. Similarly, numerical simulations have illustrated how vegetation-generated turbulence impacts the spatial distribution of suspended sediment deposition within an emergent cylinder array (e.g., Kim et al., 2018). Net deposition within a canopy also depends on the supply of sediment from the bare channel. For example, Shi et al. (2016) observed that deposition within the wake of a vegetation patch was only enhanced relative to the open channel, when resuspension was active in the channel, providing a source of suspended material to the wake. Similarly, within dense canopies, Zong and Nepf (2010) attributed regions of diminished deposition to supply limitation. Specifically, they showed that in the canopy interior ($b - \delta_p > y \geq 0$) sediment was only supplied through advection from the leading edge, and deposition along the canopy progressively reduced the suspended concentration, reducing the net deposition. Thus, even with conditions favorable for deposition (low velocity and low TKE), enhanced deposition was not observed in some parts of the canopy due to supply limitation.

The previous studies summarized above all used emergent arrays of circular stems with uniform frontal area. This study sought to advance the models for predicting velocity, turbulence, and deposition to a canopy with a more realistic morphology, *P. australis*, with non-uniform frontal area. *P. australis* has a representative morphology for emergent vegetation, with a central stem surrounded by multiple leaves, which produces a vertical variation in the frontal area.

2. Theory

2.1. Near-Bed Velocity Evolution Through *P. australis* Canopies

For an emergent canopy with uniform frontal area, velocity decreases with distance from the canopy leading edge following Equation 2. This study considered if Equation 2 could be modified to predict near-bed velocity within a canopy of non-uniform frontal area, $a = f(z)$, such as *P. australis*, Figure 1. We focused on the near-bed conditions, as these are the most relevant to sediment deposition and retention. The near-bed velocity was defined as the mean velocity in the region $0 < z < 5$ cm (labeled H_{nb} in Figure 3a), in which the local frontal area was constant (Figure 1b). The sensitivity of results on the choice of H_{nb} is discussed in Figure S2 in Supporting Information S1. Applying Equation 2, the evolution of near-bed velocity, U_{nb}, can be described as:

$$U_{nb}(x) = U_{nb(f)} + (U_{nb(0)} - U_{nb(f)})\, e^{-\frac{3x}{L_d}} \tag{4}$$

in which L_d is defined by Equation 1 using the depth-averaged frontal area, a_d, for the full water depth (H). $U_{nb(f)}$ and $U_{nb(0)}$ are the near-bed velocities in the fully developed region and at the canopy leading edge, respectively. For the *P. australis* canopies used in this study ($\phi = 0.003$–0.018), $U_{nb(0)}$ was 6%–18% smaller than the channel average velocity U_0. For simplicity, it was assumed that $U_{nb(0)} = U_0$, which is reasonable for ϕ up to 0.026 based on Figure 8 in Rominger and Nepf (2011), which shows that the velocity at the canopy leading edge is diminished by less than 10% from the upstream channel average for $\phi \leq 0.026$.

Within most natural emergent canopies, it is reasonable to assume that the bed drag is negligible compared to the canopy drag (i.e., $\frac{C_f}{C_d a_d H} \leq 2\%$, Liu & Shan, 2019; Nepf, 2012), such that within the canopy, the canopy drag balances the free surface slope, $gS = \frac{1}{2} C_d a(z) U(z)^2$. Because the energy gradient (gS) is not a function of the

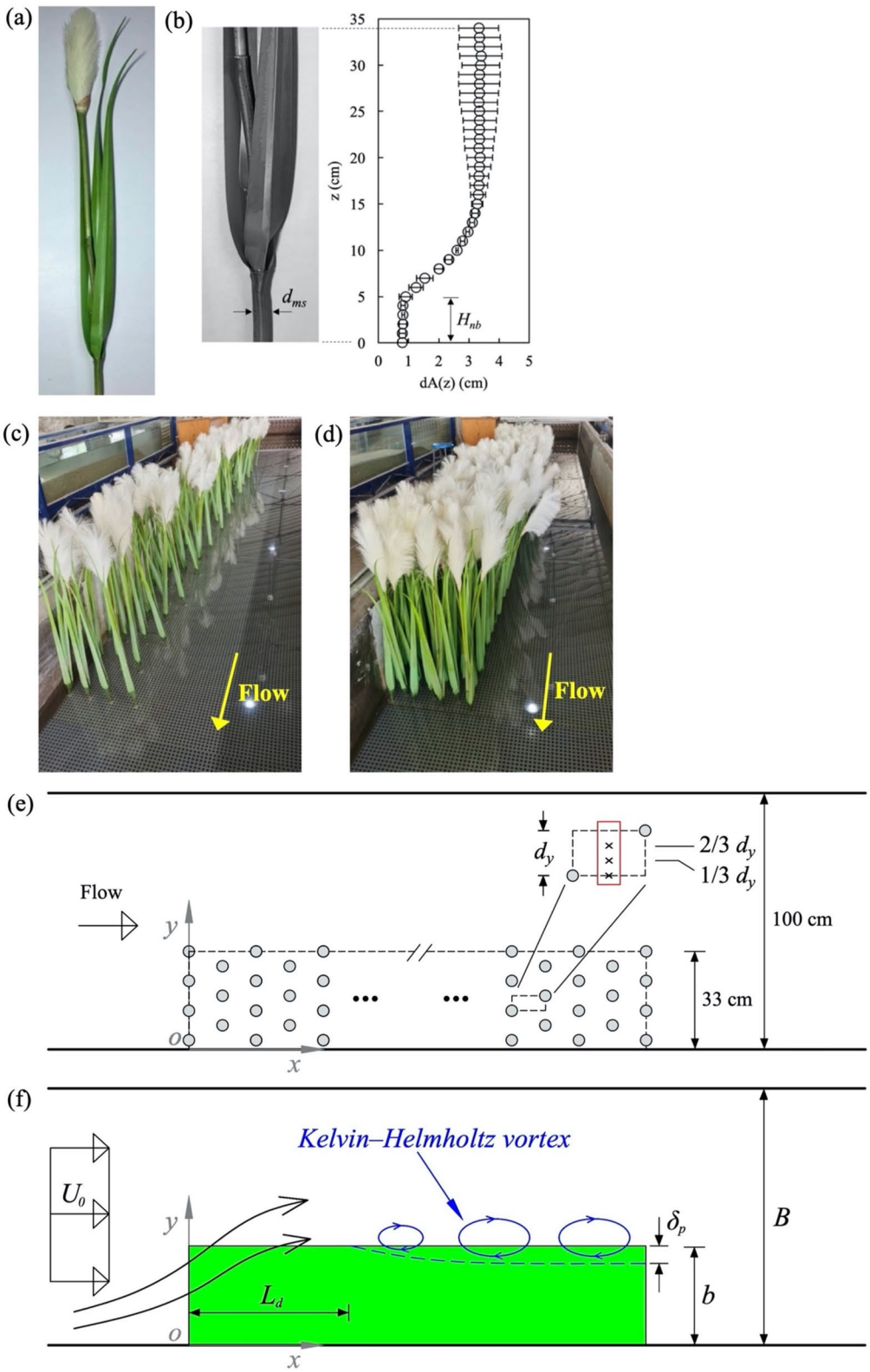
(a)
(b)
d_{ms}
z (cm)
H_{nb}
dA(z) (cm)
(c)
Flow
(d)
Flow
(e)
Flow
d_y
2/3 d_y
1/3 d_y
100 cm
33 cm
(f)
Kelvin–Helmholtz vortex
U_0
L_d
δ_p
B
b

Figure 1.

vertical coordinate (z), the drag force ($\frac{1}{2}C_d a(z)U(z)^2$) must also be vertically uniform, such that the local velocity varies inversely with the local frontal area, that is, $U(z) \propto \frac{1}{\sqrt{C_d a(z)}}$ (Lightbody & Nepf, 2006). This relation defines the near-bed velocity, $U_{nb(f)}$, relative to the depth-averaged velocity, $U_{d(f)}$. Specifically, assuming a constant C_d over the full water depth ($Z = 0$ to H) and normalizing the right-hand side of Equation 3 by a_{nb}, the frontal area per canopy volume in the near bed region (averaged over $Z = 0$ to H_{nb}):

$$U_{nb(f)} = \sqrt{\frac{a_d}{a_{nb}}} U_{d(f)} = \sqrt{\frac{2gS(1-\phi)}{C_d a_{nb}}} \tag{5}$$

in which $a_d (= nA/H)$ is the total depth-averaged frontal area, and A is the submerged frontal area of a single plant. To examine the assumption that C_d was constant over the full water depth, the measured vertical profiles of lateral-averaged streamwise velocity and local frontal area, $dA(z)$ (Figure 1b), were used to estimate the vertical profile of $C_d(z)$. Across the four cases in this study, $C_d(z)$ varied between 1.01 and 1.04 for the full water depth (Figure S3 in Supporting Information S1), indicating that it was reasonable to assume that C_d was constant over the full water depth. The assumption that C_d has only a small variation over the full water depth is also supported by previous studies (Losada et al., 2016; Shan et al., 2019; Xu & Nepf, 2020). The present study sought to verify Equations 4 and 5 for predicting near-bed velocity evolution through a canopy with non-uniform frontal area.

2.2. Near-Bed TKE Evolution Through *P. australis* Canopies

The near-bed turbulent kinetic energy per fluid mass, $k_{t(nb)}$, reflects a combination of bed-generated turbulence, $k_{t(bed)}$, and vegetation-generated turbulence, $k_{t(veg)}$. Bed-generated turbulence is related to bed shear stress, $\tau_b = \rho C_f {U_{nb}}^2$, in which ρ is the water density (Biron et al., 2004). Specifically, $k_{t(bed)} = \tau_b/\rho\omega$ with the scale constant $\omega = 0.2$ (Soulsby, 1981), suggesting that for the same near-bed velocity, a rougher channel bed (a greater C_f) generates stronger turbulence. The presence or absence of vegetation-generated turbulence depends on the stem Reynolds number, $\mathrm{Re_d}\left(= \frac{U_{nb} d_{ms}}{\nu}\right)$, in which ν is the kinematic viscosity of water, and d_{ms} is the diameter of the main stem (Figure 1b). Specifically, vegetation-generated turbulence occurs for $\mathrm{Re_d} > 120$ (Liu & Nepf, 2016). Tanino and Nepf (2008) predicted vegetation-generated turbulence inside an emergent cylinder array:

$$k_{t(veg)} = \gamma^2 \left(C_d^{form} \frac{a l_t}{2(1-\phi)} \right)^{2/3} U^2 \tag{6}$$

in which γ^2 is a scale parameter, C_d^{form} is the form drag coefficient, and l_t is the turbulent length scale. For circular cylinders, $l_t = d$ is valid for $d/s < 0.56$, in which d is the cylinder diameter and s is the cylinder spacing. The form drag is the inertial contribution to the total drag. Based on numerical simulations, Etminan et al. (2018) suggested that for $\mathrm{Re_d}\ (= Ud/\nu) > 200$, the form drag contributed 90% of the total drag on emergent cylinders; thus, it is reasonable to approximate $C_d^{form} \approx C_d$. In this study, the length scale l_t in the near-bed region ($0 < z < 5$ cm) was assumed to be the diameter of the main stem, that is, $l_t = d_{ms}$, which is supported by measurements in a canopy of *Typha latifolia*, which has a similar near-bed morphology consisting of cylindrical culms (Xu & Nepf, 2020). Finally, Yang et al. (2016) verified that the near-bed TKE in vegetated regions can be predicted by the sum of bed- and vegetation-generated turbulence, such that the near-bed TKE inside a *P. australis* canopy can be predicted as follows:

$$k_{t(nb)} = \underbrace{\frac{C_f}{\omega} {U_{nb}}^2}_{k_{t(bed)}} + \underbrace{\gamma^2 \left(C_d \frac{n {d_{ms}}^2}{2(1-\phi)} \right)^{2/3} {U_{nb}}^2}_{k_{t(veg)}} \tag{7}$$

Figure 1. (a) Image of *Phragmites australis* against a white background; (b) vertical profile of the local frontal area per cm vertical interval, $dA(z)$ ($\mathrm{cm^2/cm}$), for a single plant. The error bars indicate the variation at four rotations of three plants. d_{ms} is the diameter of the main stem. H_{nb} is the height of the near-bed region. (c) Image of a *P. australis* canopy for $n = 60$ plants/$\mathrm{m^2}$; (d) image of a *P. australis* canopy for $n = 270$ plants/$\mathrm{m^2}$; (e) sketch of the top view of the flume with a *P. australis* canopy; and (f) the sketch of flow structure inside and outside a *P. australis* canopy. Gray dots are the positions of the plants at the base. In a unit cell denoted by a dashed box, black crosses are the ADV measurement positions, and the red rectangle is the microscope glass slide that is used to collect net deposition. The lateral spacing between two rows is dy. B and b are the channel width and canopy width, respectively. L_d is the interior flow adjustment distance. δ_p is the penetration distance.

2.3. Sediment Deposition Through *P. australis* Canopies

The rate of net deposition inside a canopy may be predicted using a deposition probability model (Engelund & Fredsoe, 1976), which defines the rate of mass accumulation at the bed:

$$\frac{d\,Dep}{dt} = pw_s C \tag{8}$$

in which Dep is the net mass deposited per bed area over time duration t; p is the probability that a particle that reaches the bed remains deposited, w_s is the settling velocity of the particles, and C is the suspended sediment concentration. Because the residence time within the *P. australis* canopies (50–70 s based on canopy length and canopy-averaged velocity) was significantly shorter than the particle setting time (H/w_s = 670–1,000 s), it was reasonable to assume that the suspended sediment concentration, C, inside the canopy was equal to the sediment concentration outside the canopy. The sediment concentration was measured upstream of the canopy. The initial concentration was denoted by C_0, and the concentration C decreased over the duration of the experiment due to sediment deposition. The net deposition in the absence of resuspension ($p = 1$) was defined as $Dep_{(p=1)}$. If resuspension was present ($p < 1$), the net deposition, Dep, would be:

$$\frac{Dep}{Dep_{(p=1)}} = \frac{p}{1} \tag{9}$$

Engelund and Fredsoe (1976) provided a model for the deposition probability within a bare channel (without vegetation):

$$p = 1 - \left[1 + \left(\frac{K\pi}{6\,(\theta - \theta_c)}\right)^4\right]^{-1/4} \tag{10}$$

in which K is a friction coefficient taken to be 1, $\theta\left(=\frac{\tau_b}{(\rho_s-\rho)gd_s}\right)$ is the dimensionless shear stress (Shields parameter), with particle density, ρ_s, and θ_c is the critical Shields parameter defined by the critical bed shear stress, $\tau_{b(c)}$, needed to initiate resuspension in a bare channel. The net deposition in the bare channel (the open channel reference), $Dep_{(0)}$ ($= p \times Dep_{(p=1)}$), was estimated from Equation 9, with p estimated using bed shear stress.

In vegetated regions, the near-bed TKE, $k_{t(\mathrm{nb})}$, is the dominant factor initiating resuspension (e.g., Liu et al., 2021; Zhang et al., 2020), so the dimensionless parameter θ has been modified to reflect this contribution (see Shan et al., 2020; Zhao & Nepf, 2021):

$$\theta = \frac{\rho\omega k_{t(\mathrm{nb})}}{(\rho_s - \rho)\,g d_s} \tag{11}$$

Similarly, the critical Shields parameter can be defined as $\theta_c\left(=\frac{\rho\omega k_{t(c)}}{(\rho_s-\rho)gd_s}\right)$, with $k_{t(c)}$ the critical turbulence threshold for resuspension. As shown in Zhao and Nepf (2021), $k_{t(c)}$ can be estimated from the critical bed shear stress for bare beds, $\tau_{b(c)}$:

$$k_{t(c)} = \frac{\tau_{b(c)}}{\rho\omega} = \frac{\theta_c\,(\rho_s - \rho)\,g d_s}{\rho\omega} \tag{12}$$

3. Experimental Methods

P. australis (common reed) is the dominant emergent vegetation in many wetlands, marshes, and river deltas (e.g., Hauber et al., 2011). We employed a company to produce the plastic model plant used in this study (Figure 1a), which was similar to the aquatic plant *P. australis* having a central stem supporting panicles and leaves (Gacia et al., 2021). The main stem was surrounded by three or four leaves. The diameter of the main stem was d_{ms} = 0.8 cm. The lengths of the leaves were between 40 and 50 cm, and the leaf width was between 0.8 and 2 cm. The leaf thickness ranged from 0.3 to 0.4 mm. The plants were scaled in size to fit the test channel, so the heights of the plants ranged from 77 to 80 cm. Although the model plants were flexible and the flexibility was similar to that of real plants, reconfiguration was not observed for the velocity range (11.5–17.0 cm/s) in this study.

Table 1
Experimental Parameters[a]

Case	U_0 (cm/s)	H (cm)	N (m^{-2})	A (cm^2)	a_d (cm^{-1})	ϕ	L_d (cm)	$L_{d(p)}$ (cm)	L_{TKE} (cm)	L_{Dep} (cm)	$Dep_{(p=1)}$ (mg/cm^2)
1	11.5	30	60	78	0.016	0.004	320 ± 20	486 ± 49	27 ± 16	–	3.2 ± 0.3
2	11.5	30	270	78	0.07	0.018	250 ± 20	240 ± 17	75 ± 8	67 ± 8	2.9 ± 0.3
3	17	20	60	45	0.013	0.003	320 ± 50	453 ± 45	71 ± 10	84 ± 19	2.6 ± 0.2
4	17	20	270	45	0.062	0.015	190 ± 20	253 ± 18	84 ± 9	91 ± 7	3.2 ± 0.3

[a]U_0 is the mean channel velocity. H is the flow depth. n is the density of plants per bed area. A is the total submerged frontal area of a single plant. a_d ($= nA/H$) is the depth-averaged frontal area per volume inside the canopy. ϕ is the solid volume fraction occupied by plants. The volume of individual plants was determined by the displacement method. L_d is the measured interior flow adjustment distance inside a canopy, and $L_{d(p)}$ is the adjustment distance estimated from Equation 1 using a_d. L_{TKE} is the distance from the canopy leading edge over which near-bed TKE decreased to the critical value. L_{Dep} is the distance from the canopy leading edge over which net deposition is diminished relative to deposition outside the canopy. L_{Dep} could not be estimated in Case 1, in which reduced deposition was not observed within the canopy (Figure 5e). $Dep_{(p=1)}$ is the mean deposition in the fully developed flow region inside the canopy.

The frontal areas of individual plants were measured using image processing. Three plants were randomly chosen and photographed against a white background. For each plant, four photos were taken at different angles. Images were converted to black and white binary images using the MATLAB image processing toolbox, with black pixels denoting the plant. The pixels were converted to real distances based on a reference ruler. The frontal area in 1-cm vertical segments, $dA(z)$, with units of cm^2/cm, is shown in Figure 1b, in which $z = 0$ is the bed surface and positive upward. Horizontal bars indicate the standard deviation among different plants and rotations. The total submerged frontal area of a single plant, A, was estimated from the integral of $dA(z)$ over the flow depth ($A = \int_0^H dA(z)dz$). For a canopy with n plants per bed area, the frontal area per canopy volume is $a(z)$ ($= ndA(z)$). The depth-averaged frontal area was a_d ($= nA/H$).

The experiments were performed in a 13-m-long and 1-m-wide recirculating flume with a horizontal bed. Plastic plants were glued into PVC baseboards in a staggered arrangement covering 1/3 the channel width (Figures 1c and 1d). The PVC boards covered the entire bed, and the unfilled holes in the PVC boards were left open. Two plant densities were considered: $n = 60$ and 270 plants/m^2. Inside the canopies, plants occupied 2%–6% of the holes, such that any influence of the holes on near-bed flow structure would be the same in the canopy as over the bare bed. We designed the experiment to reach a fully developed flow within the canopy, so the canopy length was longer than the interior flow adjustment distance. For the same canopy width, a sparser canopy corresponded to a longer interior flow adjustment distance (Table 1), such that the canopy length was 4.4 m for 60 plants/m^2 and 3.0 m for 270 plants/m^2. The solid volume occupied by plants per unit water volume was determined by the displacement method, yielding the solid volume fraction $\phi = 0.003$–0.018, which was within the range of $\phi = 0.001$–0.02 observed in the field (Bellavance & Brisson, 2010; O'Hare et al., 2010; Toth & Szabo, 2012). The flow depth was measured by two rulers fixed at the leading edge and trailing edge of the canopy. Visual observation indicated that the lateral water surface slope was negligible. Two water depths, $H = 20$ and 30 cm, were considered, corresponding to channel-averaged velocities of $U_0 = 11.5 \pm 0.5$ and 17.0 ± 0.5 cm/s, respectively. The channel-average velocity was obtained from velocity profiles measured 1.5 m upstream of the canopy and at the centerline of the channel, where the flow was not influenced by the canopy. The channel Reynolds number, defined with the hydraulic radius R, was $\mathrm{Re}\left(=\frac{U_0 R}{\nu}\right) = 17,000$ to $32,000$, and the Froude number was $\mathrm{Fr}\left(=\frac{U_0}{\sqrt{gH}}\right) = 0.09$ to 0.1, indicating that the flow was turbulent and subcritical.

The coordinates x and y defined the longitudinal and lateral directions, respectively. Additionally, $x = 0$ was the leading edge of a canopy, and $y = 0$ was the right-side channel wall (Figure 1e). A Nortek Vectrino profiler was fixed on a positioning system that moved in the x, y, and z directions. The Vectrino profiler measured velocity over a 3-cm vertical span with 3-mm vertical resolution. At each position, the velocity was measured at 50 Hz for 150 s. The raw velocity data with correlations smaller than 70% and a signal-to-noise ratio less than 12 were removed, after which remaining velocity spikes were removed using the method in Goring and Nikora (2002).

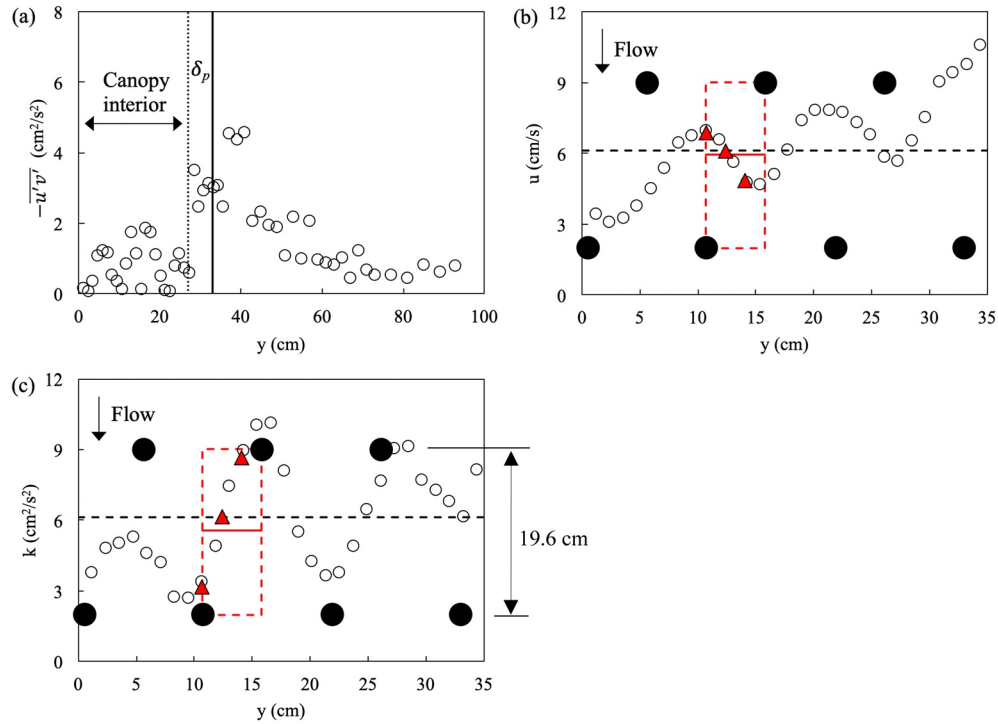

Figure 2. (a) Lateral profile of Reynolds shear stress, $-\overline{u'v'}$, across the canopy and bare channel, based on measurements from Case 3 ($H = 20$ cm, $n = 60$ plants/m^2). Velocity was measured at the midway between two rows of plants and mid-depth ($z = 10$ cm) and at $x = 2.8$ m. The vertical solid line indicates the side edge of the canopy ($b = 33$ cm). The penetration distance was $\delta_p = 6$ cm, denoted by the distance between the vertical dashed and solid lines. (b) Lateral profile of time-average velocity u, and (c) lateral profile of turbulent kinetic energy, k, inside the canopy. Black dots indicate the plant positions at the baseboard. In subplots (b and c), the horizontal dashed line indicates the laterally averaged velocity and turbulent kinetic energy (TKE) in the canopy interior, $b - \delta_p$ ($y = 0$–27 cm), respectively. The three red triangles represent three lateral measurement positions in a representative area ($y = 10.7$–15.8 cm) at each x position. The red dashed box indicates the representative area, in which the red horizontal line indicates the laterally averaged velocity, U, and laterally averaged TKE, k_t. The difference between the laterally averaged velocities and TKE in the canopy interior and the representative area was 3% and 8%, respectively.

The three components of velocity (u, v, w) were decomposed into time-averaged velocity ($\overline{u}, \overline{v}, \overline{w}$) and instantaneous fluctuations (u', v', w'). The turbulent kinetic energy is:

$$k = \frac{1}{2}\left(\overline{u'^2} + \overline{v'^2} + \overline{w'^2}\right) \tag{13}$$

A lateral profile of lateral turbulent momentum flux (Reynolds stress, $-\overline{u'v'}$) was measured at mid-depth ($z = 10$ cm) and at approximately the end of the flow adjustment region ($x = 280$ m, $L_d = 320 \pm 20$ cm). The Reynolds stress profile was used to estimate the penetration distance at the side edge of the canopy, δ_p. For the sparse canopy ($n = 60$ plants/m^2), $\delta_p = 6$ cm (Figure 2a). Note that the penetration distance evolves from zero at the leading edge of the canopy and reaches this fully-develop value at $x = L_d$, beyond which δ_p is a constant. As expected, the denser canopy ($n = 270$ plants/m^2) produced a smaller δ_p ($= 1.8\, d_{ms} = 1.4$ cm) (see Equation 9 in White & Nepf, 2008). Across all cases, the width of the canopy interior ($= b - \delta_p$) was 27.0–31.6 cm, and in this region of the canopy, the velocity and TKE were not influenced by the shear layer or KH vortices at the canopy edge. In the canopy interior, velocity was measured in the near-bed region in a representative area at $y = 10.7$–15.8 cm (close to the centerline of the canopy) at three lateral positions ($y = 10.7$, 12.4, and 14.1 cm, red triangles in Figures 2b and 2c). For the sparse and dense canopies, the lateral distance between the lines of plants remained the same, but the longitudinal distance between the rows of plants changed (Figures 1c and 1d). The representative area was repeated through the sparse and dense canopies. The laterally-averaged velocity, $U\left(=\frac{1}{3}\sum_1^3 u\right)$, and TKE, $k_t\left(=\frac{1}{3}\sum_1^3 k\right)$, within the representative unit area differed from those determined from a lateral transect across

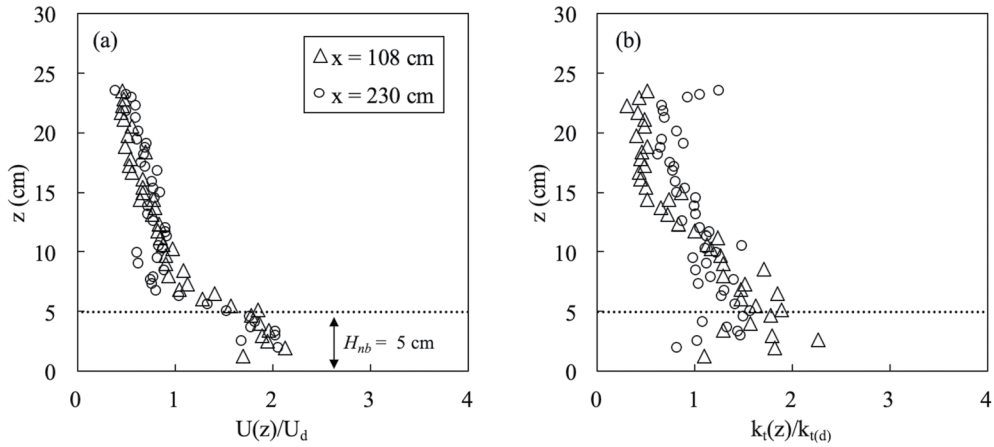

Figure 3. Vertical profiles of normalized (a) laterally averaged velocity and (b) laterally averaged turbulent kinetic energy (TKE) within the representative area inside a *Phragmites australis* canopy of $\phi = 0.018$ (Case 2, $H = 30$ cm, $U_0 = 11.5$ cm/s). U_d and $k_{t(d)}$ are the depth-averaged velocity and TKE, respectively. In Case 2, the interior flow adjustment distance was $L_d = 250 \pm 20$ cm; thus, data at $x = 108$ and 230 cm were measured approximately in the middle and at the end of the flow adjustment region, respectively. At two positions, velocity and TKE were enhanced relative to the depth-averaged values in the near-bed region ($H_{nb} = 5$ cm, denoted by the horizontal dashed line).

the full interior region of the canopy by less than 3% and 8%, respectively (Figures 2b and 2c), confirming that the representative unit area accurately captured the flow statistics in the canopy interior. In the present study, the region underneath the leaves was considered the near-bed region, that is, $H_{nb} = 5$ cm, within which the frontal area was constant in the vertical direction (Figure 1b). The near-bed velocity was $U_{nb} = \frac{1}{H_{nb}} \int_0^{H_{nb}} U(z)dz$, and the near-bed TKE was $k_{t(nb)} = \frac{1}{H_{nb}} \int_0^{H_{nb}} k_t(z)dz$. Vertical profiles of velocity over the full depth were measured at selected streamwise (x) positions and $y = 10.7$, 12.4, and 14.1 cm and used to define the full depth-averaged velocity $U_d = \frac{1}{H} \int_0^{H} U(z)dz$ within the canopy. The interior flow adjustment distance, L_d, was estimated as the distance within the canopy over which the near-bed velocity decreased to a constant within uncertainty (see Table 1). For bare beds, the Reynolds stress, that is, $-\overline{u'w'}$, was measured at $z = 1$ cm ($z/H = 0.05$) and used to estimate the bed friction coefficient. Specifically, $\tau_b \left(= \rho C_{f(bare)} U_d{}^2 = -\rho\overline{u'w'}\right)$, yielding $C_{f(bare)} = 0.005$. Inside canopies, the bed shear stress may be enhanced due to vegetation-generated turbulence, possibly enhancing the bed friction coefficient. Yang et al. (2015) proposed the estimator:

$$C_f = \max\left(C_{f(bare)}, \frac{4}{Re_d}\right) \tag{14}$$

in which $Re_d \left(= \frac{U_{nb} d_{ms}}{\nu}\right)$ is the stem Reynolds number in the near bed region. In this study, C_f ranged between 0.005 and 0.01 inside the canopies.

The drag coefficient was estimated following Etminan et al. (2017), who considered the influence of flow constriction by adjacent canopy elements. Defining the constricted near-bed velocity, $U_{nb-c} = \frac{1}{1-\sqrt{\frac{n d_{ms}{}^2}{2}}} U_{nb}$ (Etminan et al., 2017), the drag coefficient was determined from $Re_{dc} \left(= \frac{U_{nb-c} d_{ms}}{\nu}\right)$ (White, 1991, Equation 15).

$$C_d = 1 + Re_{dc}{}^{-2/3} \tag{15}$$

Across all cases, $C_d = 1.00$–1.04; thus, it is reasonable to assume $C_d = 1$ in the following prediction.

Glass spheres with a mean diameter of $d_s = 22 \pm 3$ μm were used to simulate suspended sediment. The particles had a density of $\rho_s = 2.5$ g/cm^3. The settling velocity $w_s = 0.03$ cm/s was estimated using the method of Cheng (1997):

$$\frac{w_s d_s}{\nu} = \left(\sqrt{25 + 1.2{d_*}^2} - 5\right)^{1.5} \tag{16}$$

in which $d_* \left(= \left(\frac{(\rho_s - \rho)g}{\rho\nu^2}\right)^{1/3} d_s = 0.54\right)$ is the dimensionless particle diameter. The model particle was selected to achieve a ratio of settling velocity to bare channel critical shear velocity that fell within the range observed for fine organic matter in streams ($w_s/u_* = 0.002$–0.03, see discussion in Ortiz et al., 2013). Using $u_* = \sqrt{C_f}U_0$, the experimental conditions fell in the range ($w_s/u_* = 0.025$–0.037). For $d_* = 0.3$–19, $\tau_{*c} = 0.25{d_*}^{-0.6}\tan 30° = 0.21$ (Julien, 2010). Finally, the critical turbulence threshold, $k_{t(c)} = 3.4 \pm 0.2$ cm^2/s^2, was estimated by Equation 12.

The deposition experiments were conducted separately from velocity measurements to avoid having the velocity probe interfere with deposition. Rectangular slides (2.5 × 7.5 cm) were placed along the centerline of the canopy. Slides were also placed >0.5 m upstream of the canopy to obtain net deposition in the bare channel. The slides were weighed before placement in the flume. Once placed, the pump valve was slowly opened until the target mean channel velocity was achieved. The model particles were mixed with water in a measuring cup, and the slurry was gently added to the downstream tank. The recirculating pump transported the water and particles to the upstream tank. As the sediment passed through the pump, it was mixed to a uniform concentration, such that the suspended sediment concentration was always vertically uniform at the upstream end of the channel. The water and particles were completely mixed over the depth and width of the flume within 2 min. In each case, the initial concentration ($C_0 = 100$ g/cm^3) was estimated from the added particle mass and the water volume in the flume and tanks. Once a uniform concentration was achieved, the deposition experiment ran for 4 hr. Deposition was insufficient to form a sediment bed during the experiment, so bedforms were not observed. After 4 hr, the pump was slowly turned down to prevent the formation of surface waves. Four additional slides were gently placed in the bare channel to measure the net deposition during draining. The water was slowly drained, which took 25 min. Afterward, the slides were left to dry in the flume for 1 day. Once dry, the slides were carefully removed from the channel bed and placed in an oven at 40°C for 8 hr to remove the remaining moisture. The slides were reweighed, and the net deposition at each position was the weight difference before and after the experiment. Each case was repeated to estimate the uncertainty in the net deposition. The net deposition at $x = -120$ cm (upstream of the canopy) was considered to be the open channel reference, denoted as $Dep_{(0)}$. For $U_0 = 11.5$ cm/s (Cases 1 and 2) and $U_0 = 17$ cm/s (Cases 3 and 4), $Dep_{(0)} = 3.3 \pm 0.5$ and 1.9 ± 0.3 mg/cm^2, respectively.

In the absence of resuspension, such that $p = 1$, the net deposition that can occur over the duration of the experiment, t, is defined as

$$Dep_{(p=1)} = w_s \int_0^t C(t)dt \tag{17}$$

Pure deposition was observed in Case 1 (i.e., no resuspension, see Section 4.2), so the average net deposition along the entire channel for this case was assumed to define $Dep_{(p=1)}$ (= 3.2 ± 0.3 mg/cm^2, Table 1). To facilitate comparisons, deposition measurements in each case were normalized by this pure deposition (3.2 ± 0.3 mg/cm^2). Given that the mass addition, and thus C_0, the settling velocity, w_s, and experiment duration, t, is the same for each experiment, it is reasonable to assume that the pure deposition limit $Dep_{(p=1)}$ is also the same in the four cases (Equation 17), which is confirmed in Table 1.

The pure deposition in Case 1 was also used to estimate net deposition in the head and tail tanks of the channel. The total deposition on the channel bed (13 m^2) and the tank bottoms (4 m^2) was 561 g (= 3.3 mg/cm^2 × 17 m^2), which was 93% of the added mass (605 g), indicating that only 7% of the added particles were lost in the pipe system. Given this, it is reasonable to ignore the impact of deposition in the pipe system on the experimental results.

To compare the total particle retention in the canopies, we defined an average deposition per bed area by integrating over the canopy length, L, and normalizing by the maximum deposition defined by pure deposition, $Dep_{(p=1)}$.

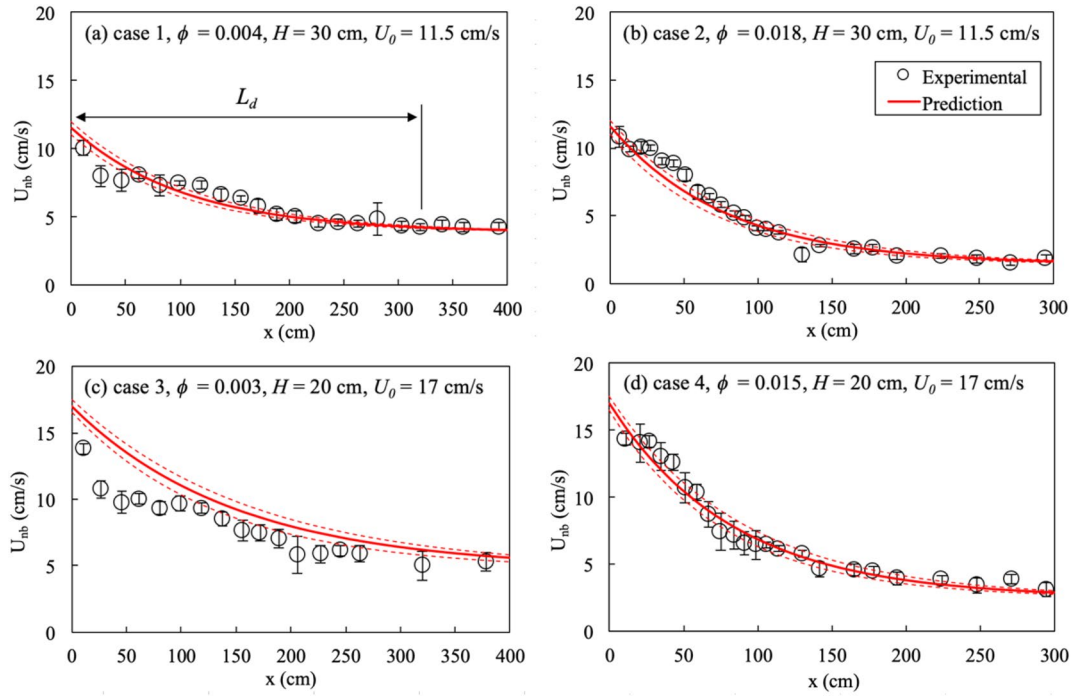

Figure 4. Predicted near-bed velocity, U_{nb}, estimated from Equations 4 and 5, compared with measurements within *Phragmites australis* canopies. L_d is defined as the flow adjustment distance over which the near-bed velocity decreases to a constant, as shown in subplot (a). Case 1 had a measured $L_d = 320 \pm 20$ cm. Dashed lines are the propagated uncertainty in U_0 and L_d. Canopy density and flow conditions were denoted in each subplot. The uncertainty in U_{nb} was the standard derivation of velocities in the near-bed region (z = 0–5 cm). The noise in the velocity measurements was 0.2 cm/s, which was generally smaller than the uncertainty in U_{nb}.

$$M_{canopy} = \frac{1}{L}\int_0^L \frac{Dep(x)}{Dep_{(p=1)}}dx = \frac{1}{L}\int_0^L p dx \tag{18}$$

For the bare-bed, the same non-dimensional mass deposited per bed area was

$$M_{bare} = \frac{Dep_{(0)}}{Dep_{(p=1)}} \tag{19}$$

4. Results

4.1. Near-Bed Velocity and TKE

In the near-bed region underneath the leaves ($z < H_{nb} = 5$ cm, Figure 1), the velocity and TKE were approximately constant in the vertical direction (Figure 3), so it was reasonable to define the near-bed velocity, U_{nb}, and near-bed TKE, $k_{t(nb)}$, as the vertical average in this region. Using the depth-averaged frontal area, a_d, Equation 1 predicted the measured flow adjustment distance, L_d, to within 34% (Table 1), indicating that Equation 1 is a useful estimator for the flow adjustment distance inside canopies with natural morphology. The predicted $L_{d(p)}$ was used with Equations 4 and 5 to predict near-bed velocity evolution (Figure 4), which agreed with measured values to within an average relative error of 12%.

The predicted near-bed velocity was used to predict near-bed TKE (Equations 7 and 14), which was compared to the measured TKE in Figures 5a–5d (left side images). Using the enhanced bed friction coefficient, C_f, expected within the canopies (Equation 14), the scale constant $\gamma^2 = 1.3 \pm 0.2$ (95% CI) was estimated based on a least-squares fit between the predicted and measured $k_{t(nb)}$ for all cases in Table 1. This scale constant agreed within uncertainty with the constant observed in an emergent cylinder array ($\gamma^2 = 1.2$, Tanino & Nepf, 2008) and a canopy of the model *T. latifolia* ($\gamma^2 = 1.6 \pm 0.4$, Xu & Nepf, 2020). In the near-bed region, the main stem of *P. australis* was simi-

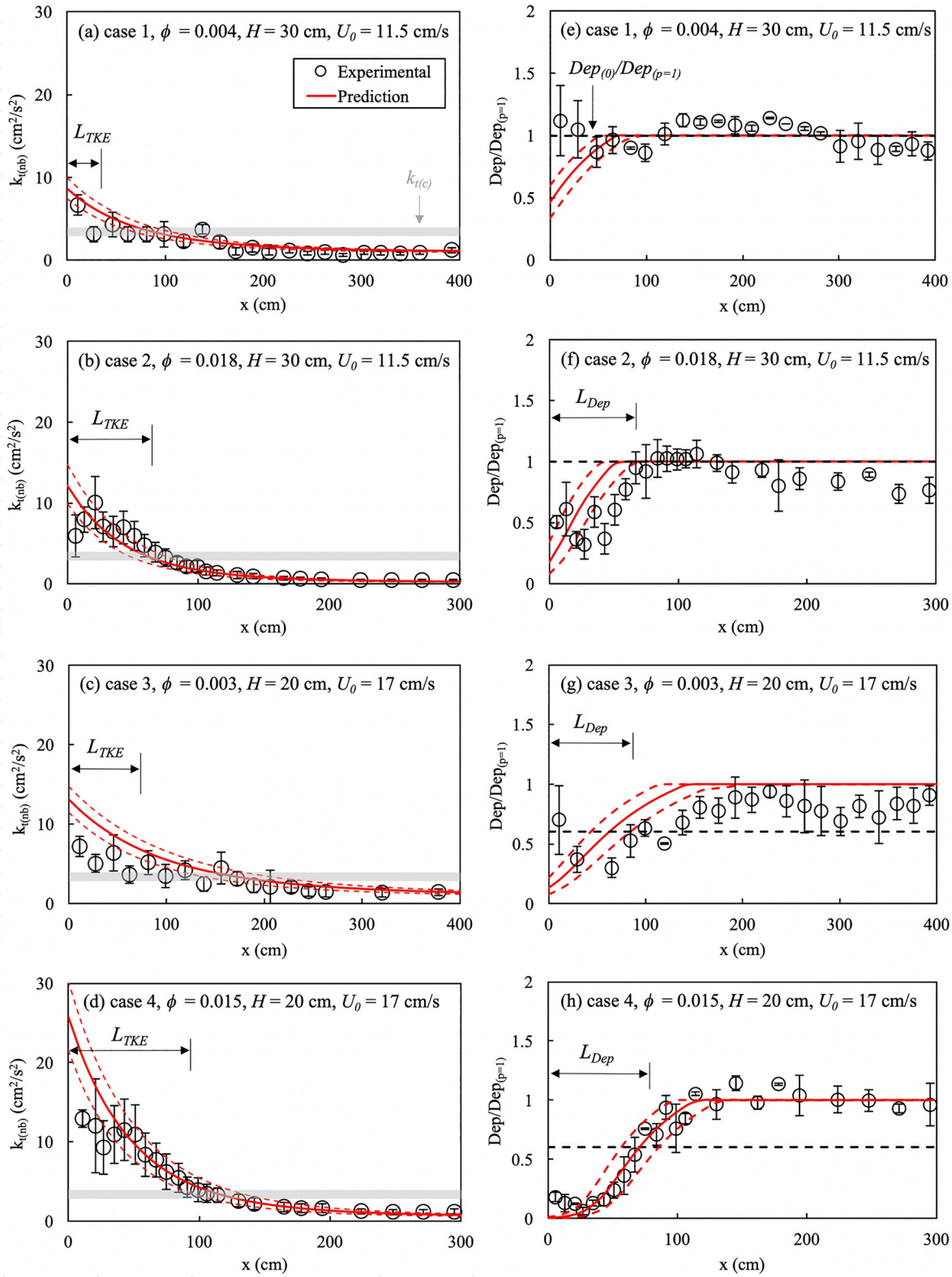
(a) case 1, ϕ = 0.004, H = 30 cm, U_0 = 11.5 cm/s
Experimental
Prediction
L_{TKE}
$k_{t(c)}$
$k_{t(nb)}$ (cm^2/s^2)
x (cm)
(b) case 2, ϕ = 0.018, H = 30 cm, U_0 = 11.5 cm/s
(c) case 3, ϕ = 0.003, H = 20 cm, U_0 = 17 cm/s
(d) case 4, ϕ = 0.015, H = 20 cm, U_0 = 17 cm/s
(e) case 1, ϕ = 0.004, H = 30 cm, U_0 = 11.5 cm/s
$Dep_{(0)}/Dep_{(p=1)}$
Dep/Dep$_{(p=1)}$
(f) case 2, ϕ = 0.018, H = 30 cm, U_0 = 11.5 cm/s
L_{Dep}
(g) case 3, ϕ = 0.003, H = 20 cm, U_0 = 17 cm/s
(h) case 4, ϕ = 0.015, H = 20 cm, U_0 = 17 cm/s

Figure 5.

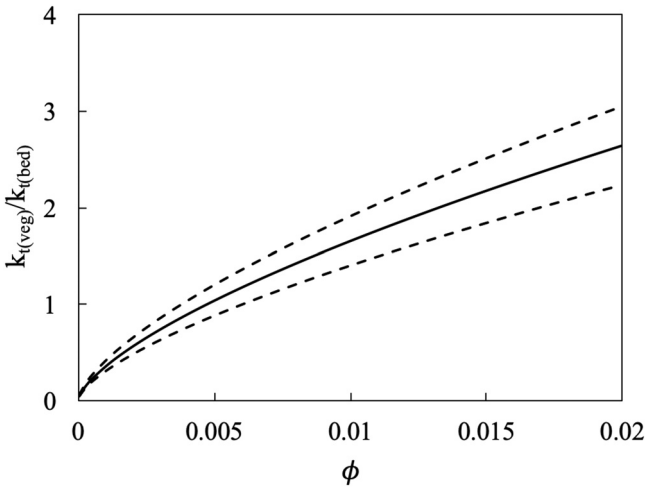

Figure 6. The ratio of vegetation-generated turbulence to bed-generated turbulence, $k_{t(veg)}/k_{t(bed)}$, predicted by Equation 7, versus solid volume fraction, ϕ. Two dashed lines indicate the uncertainty in γ^2.

lar to a circular cylinder, such that it is reasonable to use $\gamma^2(= 1.2)$ based on an emergent cylinder array for *P. australis*. If $C_f = C_{f(bare)}$ was assumed across all cases, γ^2 increased by 15%, and this percentage was within the uncertainty. For simplicity, $C_f = 0.005$ was used for all cases. The predicted near-bed TKE reproduced the measured streamwise evolution of TKE within the canopy (red lines in Figures 5a–5d). Given the good agreement between the measured and predicted TKE, Equation 7 can be used to compare the relative contributions of bed-generated turbulence ($k_{t(bed)}$) and vegetation-generated turbulence ($k_{t(veg)}$) within the *P. australis* canopy (Figure 6). The vegetation-generated turbulence is dominant for $\phi > 0.005$. Natural *P. australis* canopies have $\phi = 0.001$–0.02 (Bellavance & Brisson, 2010; O'Hare et al., 2010; Toth & Szabo, 2012), which includes conditions in which bed-generated turbulence dominates ($\phi < 0.005$) and in which vegetation-generated turbulence dominates ($\phi > 0.005$). Therefore, for natural canopies, both contributions must be included for predicting near-bed TKE.

4.2. Sediment Deposition

The net deposition inside the *P. australis* canopies was dependent on both the mean channel velocity and plant density. First, consider the low-velocity Cases 1 and 2 ($U_0 = 11.5$ cm/s). For the low-density case (Case 1, $n = 60$ plants/m^2), the net deposition was spatially uniform throughout the canopy and equal to the deposition upstream of the canopy, $Dep_{(0)}$ ($= 3.3 \pm 0.5$(SD) mg/cm^2, denoted by a horizontal black dashed line in Figure 5e). These observations suggested that the conditions in Case 1 produced pure deposition over the entire channel; that is, resuspension was absent. This was consistent with the fact that the measured turbulence was below the predicted critical TKE needed to initiate resuspension at all locations, except the first point at the canopy leading edge ($k_{t(c)} = 3.4 \pm 0.2$ cm^2/s^2, shown with horizontal gray bar in Figure 5a). For the same channel velocity but higher plant density ($n = 270$ plants/m^2, Case 2, Figure 5f), the net deposition was diminished near the leading edge and over a distance L_{Dep} relative to $Dep_{(0)}$ (horizontal black dashed line), which was attributed to near-bed TKE higher than $k_{t(c)}$ close to the canopy leading edge (Figure 5b). Beyond $x = L_{Dep}$, deposition became uniform and equal to $Dep_{(0)}$ within uncertainty (Figure 5f), suggesting that resuspension was absent, which was consistent with TKE falling below $k_{t(c)}$ in this region (Figure 5b). Next, consider the high-velocity Cases 3 and 4 ($U_0 = 17$ cm/s), for which net deposition in the canopy was both elevated above and diminished below the deposition outside the canopy, $Dep_{(0)}$ (Figures 5g and 5h). Specifically, deposition was reduced over distance L_{Dep} and enhanced beyond L_{Dep}, relative to deposition outside the canopy, $Dep_{(0)}$ (horizontal black dashed line). Importantly, for the higher velocity cases, deposition outside the canopy ($Dep_{(0)} = 1.9 \pm 0.3$ mg/cm^2) was reduced compared to the pure deposition (3.3 ± 0.5 mg/cm^2), which indicated that resuspension was present outside the canopy, making more particles available to enter and deposit inside the canopy. As a result, regions within the canopy with near-bed TKE smaller than $k_{t(c)}$ ($x > 80$ and 90 cm, Figures 5c and 5d, respectively) were associated with net deposition that was enhanced relative to $Dep_{(0)}$ outside of the canopy ($x > 80$ and 90 cm, Figures 5g and 5h, respectively). Closer to the canopy leading edge ($x < 80$ cm), the near-bed TKE was both greater than $k_{t(c)}$ (Figures 5c and 5d) and also greater than the bare bed (4.7 ± 0.3 cm^2/s^2). Higher TKE resulted in more intense resuspension in this region of the canopy, compared to the bare bed, driving the net deposition below the bare bed value $Dep_{(0)}$ (Figures 5g and 5h).

L_{TKE} was defined as the distance from the canopy leading edge over which near-bed TKE decreased to $k_{t(c)} = 3.4 \pm 0.2$ cm^2/s^2 (Figures 5a–5d, Table 1). L_{Dep} was defined as the distance from the canopy leading edge over which net deposition was diminished relative to outside the canopy (Figures 5e–5h, Table 1). These length scales were the same within uncertainty ($L_{Dep} = L_{TKE}$, Table 1), supporting that turbulence controls the

Figure 5. (a–d) Predicted near-bed turbulent kinetic energy (TKE), $k_{t(nb)}$, estimated from Equation 7, compared with measurements. The scale constant $\gamma^2 = 1.3 \pm 0.2$ (95% CI) was determined by a least-squares fit of predicted $k_{t(nb)}$ to measurements from all Cases in Table 1. Dashed lines are the propagated uncertainty in U_{nb} and γ^2. L_{TKE} indicates the distance from the canopy leading edge over which the near-bed TKE exceeds the critical turbulence level for resuspension ($k_{t(c)} = 3.4 \pm 0.2$ cm^2/s^2, estimated from Equation 12, denoted by horizontal bars). (e–h) Predicted normalized deposition, $Dep/Dep_{(p=1)}$, compared with measurements. Dashed red lines denote the uncertainty in predictions. Net deposition outside canopies, $Dep_{(0)}$, normalized by the pure deposition, $Dep_{(p=1)}$, is denoted by horizontal black dashed lines. L_{Dep} is the distance from the canopy leading edge over which deposition was diminished relative to $Dep_{(0)}/Dep_{(p=1)}$. The noise in the TKE measurements was 0.3 cm/s.

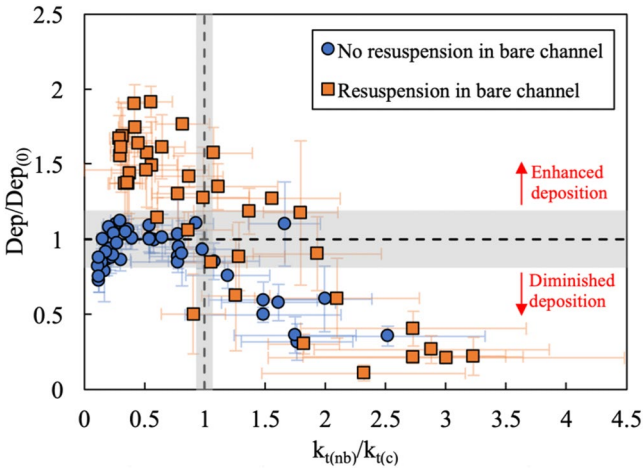

Figure 7. The net deposition within the canopy relative to the deposition upstream of the canopy, $Dep/Dep_{(0)}$, against the near-bed turbulent kinetic energy normalized by the critical turbulence level for resuspension, $k_{t(nb)}/k_{t(c)}$, for no resuspension (Cases 1 and 2, blue circles) and resuspension (Cases 3 and 4, orange squares) in the bare channel. The horizontal gray bar indicates $Dep/Dep_{(0)} = 1$, and its width reflects the uncertainty in $Dep_{(0)}$. The resuspension threshold $k_{t(nb)}/k_{t(c)} = 1$ is marked by a vertical bar, and its width indicates the uncertainty in $k_{t(c)}$. $Dep/Dep_{(0)} > 1$ and <1 indicate net deposition greater than or smaller than the upstream referred deposition, respectively.

resuspension, and thus the net deposition, and confirming the prediction of the critical turbulence level, $k_{t(c)}$. For the same channel velocity, L_{TKE} increased with plant density (n), consistent with Equation 7. For the same plant density, larger channel velocity (resulting in larger U_{nb}) produced longer L_{TKE}, which was also consistent with Equation 7.

Because enhanced net deposition within a canopy can impact nutrient budgets, seed capture, and carbon accretion, there is interest in understanding the conditions needed for enhanced net deposition to occur within a canopy, relative to bare channel. Net deposition in the canopy normalized by the bare channel value, $Dep/Dep_{(0)}$, was plotted versus the near-bed TKE normalized by the critical turbulence level for resuspension, $k_{t(nb)}/k_{t(c)}$ (Figure 7). The symbol color indicates whether resuspension was (orange, $Dep_{(0)} < Dep_{(p=1)}$) or was not (blue, $Dep_{(0)} = Dep_{(p=1)}$) present in the open channel. The threshold $Dep/Dep_{(0)} = 1$ is shown with a horizontal bar, and its width reflects the uncertainty in $Dep_{(0)}$. The resuspension threshold $k_{t(nb)}/k_{t(c)} = 1$ is marked by a vertical bar, and its width indicates the uncertainty in $k_{t(c)}$. Enhanced deposition ($Dep/Dep_{(0)} > 1$) was observed when resuspension was active in the channel (orange points), and turbulence in the canopy was below the critical threshold ($k_{t(nb)}/k_{t(c)} < 1$). When these two criteria are satisfied, enhanced deposition is observed inside the canopy because the active resuspension outside the canopy provides more sediment to be available for deposit inside the canopy. A similar observation was made by Shi et al. (2016) but framed in terms of bed stress. Specifically, they observed enhanced deposition in the wake of a vegetation patch only when the bed stress exceeded the critical value for resuspension in the channel, but not in the wake. The present study refines these criteria for conditions within the canopy by framing the observations in terms of the critical turbulence level. It is important to emphasize that, when near bed turbulence was above the critical value, $k_{t(nb)}/k_{t(c)} > 1$ in the canopy, the net deposition in the canopy was always diminished relative to the open channel ($Dep/Dep_{(0)} < 1$ in Figure 7) whether, or not, resuspension was active in the open channel (i.e., for both blue and orange points in Figure 7). This occurred primarily near the leading edge of the canopy before the in-canopy velocity was fully decelerated. When resuspension was absent in the bare channel (blue circles), enhanced deposition (relative to the open channel) was never observed in the canopy, highlighting the importance of resuspension in the channel.

The TKE evolution predicted from Equation 7 and $k_{t(c)}$ estimated from Equation 12 was inserted into Equations 9–11 to predict the distribution of net deposition, shown with red lines in Figures 5e–5h. For the majority of points, the predicted and measured deposition agreed within uncertainty. This validated the idea that the deposition probability could be defined by near-bed TKE, providing a reasonable way to predict the net deposition inside canopies.

5. Discussion

5.1. Comparison of the Bed Shear Stress Model and Near-Bed TKE Model

In bare channels, deposition and resuspension are classically modeled in terms of bed shear stress (e.g., Engelund & Fredsoe, 1976). However, previous studies have shown that bed shear stress is not a good predictor of bed load transport within vegetation canopies (e.g., Yager & Schmeeckle, 2013; Yang et al., 2016). It is useful to consider the application of bed-stress models in predicting the net deposition patterns within canopies. Specifically, we compared the net deposition predicted from the deposition probability p in Equation 9, with θ and θ_c estimated from bed shear stress (τ_b) and from near-bed TKE ($k_{t(nb)}$). The methods are denoted the τ_b-model and TKE-model, respectively. Note that the τ_b-model includes the influence of stem-turbulence on bed friction coefficient (Equation 14). Consider Case 4 (Figure 8, $H = 20$ cm, $U_0 = 17$ cm/s, $\phi = 0.015$). The bed shear stress was estimated as $\tau_b = \rho C_f U_{nb}^2$, and the near-bed TKE was estimated from Equation 7. The critical shear stress, $\tau_{b(c)}$, and critical TKE, $k_{t(c)}$, for initiating resuspension were estimated from the Shields parameter and Equation 12, respectively. The bed shear stress fell below $\tau_{b(c)}$ at $x = 40$ cm, which was closer to the canopy leading edge than the position

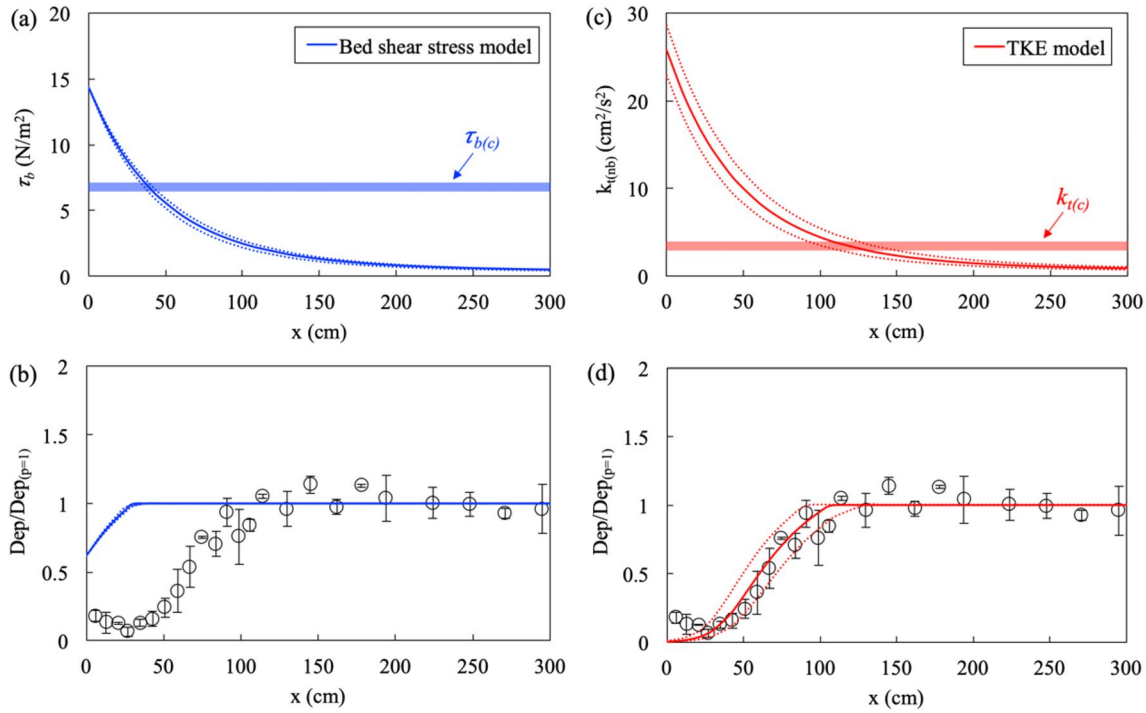

Figure 8. (a, c) Longitudinal profiles of bed shear stress, estimated from $\tau_b = \rho C_f U_{nb}^2$, and near-bed turbulent kinetic energy (TKE), estimated from Equation 7. In the two subplots, $\tau_{b(c)}$ (= 6.8 ± 0.4 N/m^2) and $k_{t(c)}$ (= 3.4 ± 0.2 cm^2/s^2) are the critical shear stress and critical TKE for initiating resuspension, respectively, estimated from Equation 12. (b, d) Net deposition, *Dep*, normalized by the pure deposition, $Dep_{(p=1)}$. $Dep/Dep_{(p=1)}$ was estimated from the bed shear stress model and TKE model, respectively, based on Equation 9. The experimental data were from Case 4 (H = 20 cm, U_0 = 17 cm/s, ϕ = 0.015).

at which TKE fell below $k_{t(c)}$ at x = 120 cm (Figures 8a and 8c). As a result of this difference, the τ_b-model and TKE-model produced different longitudinal profiles of deposition (Figures 8b and 8d). The TKE-model had good agreement with the measurements (symbols), but the τ_b-model overestimated deposition near the canopy leading edge. This was because the bed shear stress model did not reflect the contribution of vegetation-generated turbulence, which is particularly important at the leading edge. Note that in the fully developed region of the canopy (x > 100 cm), p = 1 was predicted by both models, so that both models predicted pure deposition ($Dep/Dep_{(0)}$ = 1). However, for a higher in-canopy velocity in the fully developed region, it would be possible for $k_{t(veg-f)}/k_{tc} > 1$ while $\tau_b/\tau_{b(c)} < 1$, such that the TKE-model would accurately predict resuspension but the τ_b-model would not, resulting in an overprediction of net deposition by the τ_b-model, as observed at the leading edge.

Canopy density can also influence the performance of the τ_b-model in comparison to the TKEmodel. Consider Case 4 shown in Figure 8. For this vegetation density (ϕ = 0.015), vegetation-generated turbulence was two times greater than bed-generated turbulence (Figure 6). Given this, it makes sense that the TKEmodel gave a more accurate prediction than the bed shear stress model at the leading edge. However, if the plant density was sufficiently low (e.g., ϕ = 0.001), such that the bed-generated turbulence was significantly greater than the vegetation-generated turbulence (Figure 6), the τ_b-model and TKE-models would converge, and the bed shear stress would provide a reasonable estimation of the deposition distribution. To recap, the τ_b-model includes the influence of stem-turbulence on bed friction coefficient (Equation 14), which enhances bed shear stress, and thus enhances bed-generated turbulence within the canopy. Further, because bed shear stress and bed-generated turbulence are correlated, the τ_b-model reflects the impact of bed-generated turbulence on resuspension. However, the τ_b-model does not reflect the direct impact of stem-generated turbulence on resuspension. For this reason, when stem-generated turbulence exceeds bed-generated turbulence ($\phi > \approx 0.01$, Figure 4 in Yang & Nepf, 2019), the TKEmodel is a better choice for predicting resuspension.

Because the TKEmodel can accurately capture the deposition distribution inside a realistic canopy, the TKEmodel was used to examine the influence of plant morphology (plant species) on deposition. Specifically, predictions of velocity, TKE, and deposition were made for three species of aquatic vegetation (*Rotala indica*, *T. latifolia*,

and *P. australis*). The vertical profile of the frontal area for each species is shown in Figure S1a in Supporting Information S1. *P. australis* and *T. latifolia* have vertically varying frontal areas, and *R. indica* has a vertically uniform frontal area. Longitudinal profiles of near-bed velocity, near-bed TKE, and deposition are plotted for three canopies (Figure S1 in Supporting Information S1). For the same canopy-average solid volume fraction, the spatial distribution of deposition inside the canopies with variable frontal area (*P. australis* and *T. latifolia*) was similar to that predicted for vertically uniform canopy (*R. indica*, Figure S1d in Supporting Information S1). This comparison suggested that, assuming the same solid volume fraction, the plant morphology (plant species) may have little impact on deposition distribution within an emergent canopy. Given this, for emergent canopies, a reasonable prediction of deposition can be made simply using a vertically-average frontal area. Consistent with this, the definition of the near-bed region height had an insignificant impact on deposition. Specifically, within the *T. latifolia* canopy, the predicted deposition using three values of near-bed region height (H_{nb} = 2, 5, and 8 cm) were the same within uncertainty, suggesting that the height of the near-bed region height had only a weak influence on the predicted deposition (Figure S2 in Supporting Information S1).

5.2. Critical ϕ for Enhanced Deposition Inside Canopies

Having validated a model predicting deposition within a vegetation canopy (Figure 5), the model was used to determine the critical solid volume fraction, ϕ_c, above which the spatially-averaged deposition inside a *P. australis* canopy can surpass that in a bare channel, that is, for which $M_{canopy} > M_{bare}$. As an example, we considered water depth H = 20 cm, canopy width b = 33 cm, and canopy length L = 300 cm. This canopy size is within the range of canopy width (20–400 cm) and length (20–700 cm) observed in streams (e.g., Cornacchia et al., 2018; Cotton et al., 2006). The critical solid volume fraction was determined using Equations 18 and 19 for two channel-average velocities (U_0 = 17 and 25 cm/s) and three sediment sizes (10, 22, and 40 μm). Resuspension was active in the bare channel for all conditions. Canopy-averaged deposition, M_{canopy} (solid lines in Figure 9), was predicted from Equation 18 using Equation 10 and predicted near-bed TKE. The bare channel deposition, M_{bare} (horizontal bar in Figure 9), was predicted from Equation 19 using Equation 10.

First, Figure 9a compares two velocities (U_0 = 17 and 25 cm/s, d_s = 22 μm). The value of M_{canopy} measured in Case 4 (red circle in Figure 9a) agreed with the corresponding prediction (red curve in Figure 9a). Within uncertainty, the critical solid volume fraction for U_0 = 17 cm/s (ϕ_c = 0.0019 ± 0.0008) was the same as that for U_0 = 25 cm/s (ϕ_c = 0.0017 ± 0.0002), suggesting that ϕ_c was not a function of channel-average velocity. This makes sense because ϕ_c is associated with the condition producing the same TKE (and thus the same deposition probability) in the canopy as in the bare channel. Since the ratio of $k_{t(veg-f)}$ (Equations 5 and 7) to $k_{t(bare)}$ ($= C_f U_0^2/\omega$) is not a function of channel-average velocity (Figure 9b), neither is value of ϕ_c, which is defined by the ratio $k_{t(veg-f)}/k_{t(bare)} = 1$. Similarly, since the ratio $k_{t(veg-f))}/k_{t(bare)} = 1$ is not a function of sediment size, the critical density, ϕ_c, also had no dependence on sediment size. Specifically, as sediment size increased, $k_{t(c)}$ increased, so that the deposition probability increased, and both M_{canopy} and M_{bare} increased. However, ϕ_c = 0.0017 ± 0.0002 was unchanged (Figure 9c).

The canopy length can influence ϕ_c (Figure 9d). Consider U_0 = 25 cm/s as an example (the blue line in Figure 9d). For canopy lengths less than 120 cm, all values of ϕ produced in-canopy TKE greater than the bare channel over the entire canopy length, such that enhanced deposition inside the canopy was not possible. However, for L > 120 cm, enhanced deposition was possible within the canopy, because beyond this canopy length (120 cm), in-canopy turbulence dropped below the bare channel value. Because the length-scale of flow adjustment, L_d, increases as ϕ decreases, as the canopy length increases, regions of deposition can occur within the canopy at lower values of ϕ_c (Figure 9d). Since the onset of in-canopy deposition is related to flow adjustment distance, the ratio of canopy length to the flow adjustment distance, L/L_d, was plotted for each ϕ_c (Figure 9e). Across all ϕ_c, condition $L/L_d > 0.4$ defines when the enhanced deposition was possible, because for this canopy length ($L > 0.4L_d$), the velocity and turbulence inside the canopy decreased sufficiently to enhance deposition, compared to the bare channel.

Note that the above analysis assumed that there was no supply limitation within the canopy. Specifically, the advection time scale through the canopy ($= L/U_{f(nb)}$ = 8–50 s) was much shorter than the particle settling time ($= H/w_s$ = 210–3300 s). However, a sediment supply limitation may exist for denser and/or longer canopies, for which the advection time scale is comparable to or longer than the settling time scale.

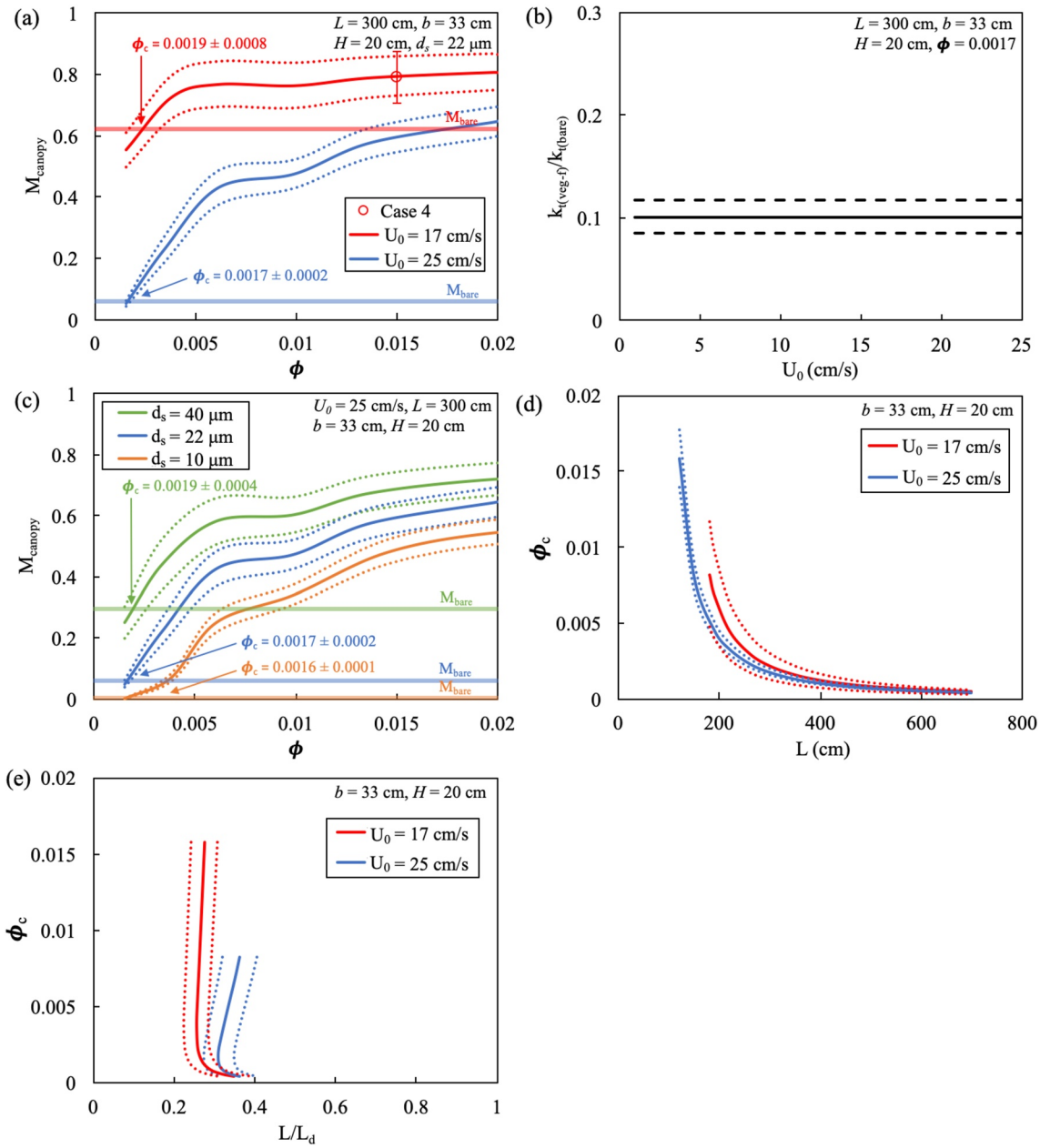

Figure 9. (a) Canopy-averaged deposition normalized by the pure deposition, M_{canopy} (Equation 18), against the solid volume fraction, ϕ, for two channel-average velocities $U_0 = 17$ and 25 cm/s. M_{bare} is the deposition per bed area in the bare channel, normalized by pure deposition (Equation 19). As a reference, Case 4 is shown with a red circle, confirming agreement with the predicted M_{canopy} (red line in Figure 10a). The critical solid volume fraction, ϕ_c, was defined as the smallest solid volume fraction for which M_{canopy} exceeded M_{bare}. (b) The ratio of near-bed turbulent kinetic energy (TKE) in the fully developed flow region of the canopy to bare channel TKE, $k_{t(veg-f)}/k_{t(bare)}$, against channel-average velocity. (c) M_{canopy} versus ϕ for three sediment sizes $d_s = 10$, 22, and 40 μm. (d) Critical solid volume fraction, ϕ_c, against canopy length for two channel-average velocities. (e) Canopy length, normalized by flow adjustment distance, L/L_d, for each ϕ_c. In each subplot, the flow, canopy, and sediment conditions are shown in the top right corner. Resuspension is present in the bare channel.

5.3. Depth-Averaged Velocity Model

Many river models are 2-D, considering only the depth-averaged velocity. Therefore, it is of practical interest to consider whether deposition can be predicted using the depth-averaged velocity, denoted by $\langle\rangle_d$. Adjusting Equation 2 for depth-averaged velocity:

$$\langle U\rangle_d = \langle U_{(f)}\rangle_d + (U_{(0)} - \langle U_{(f)}\rangle_d)\, e^{-\frac{3x}{L_d}} \tag{20}$$

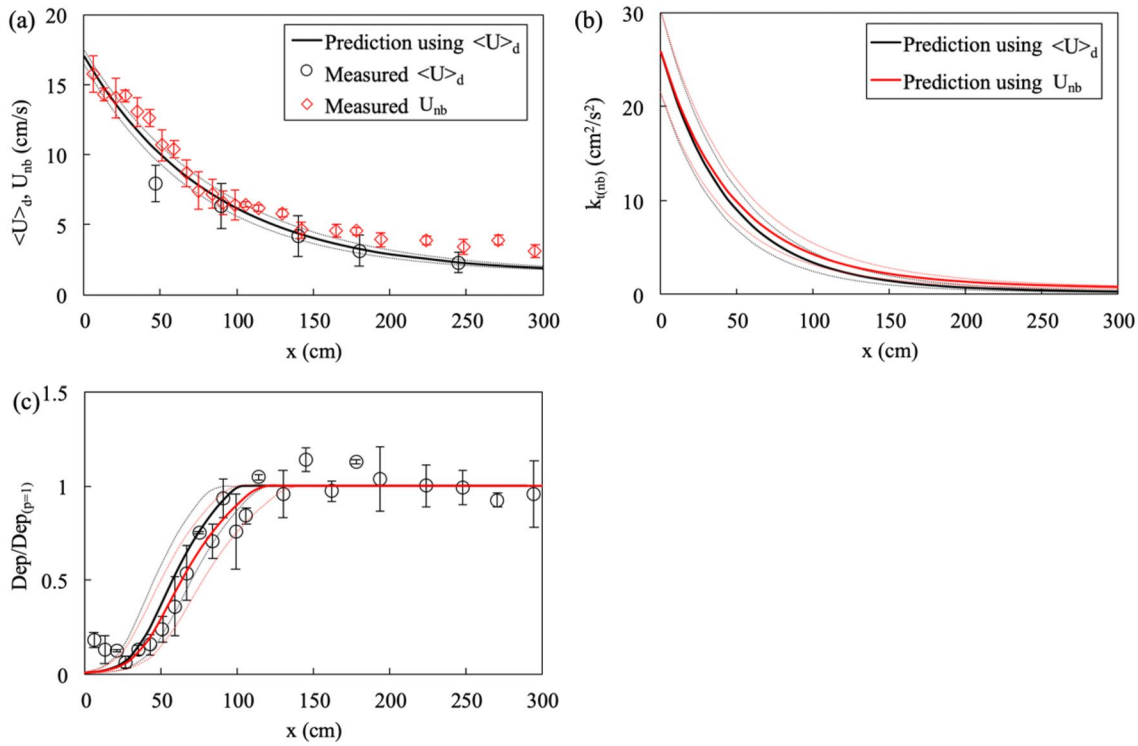

Figure 10. (a) Longitudinal profile of depth-averaged velocity, $\langle U \rangle_d$ (predicted by Equation 20), compared to the measured $\langle U \rangle_d$ and near-bed velocity, U_{nb}. (b) Near-bed turbulent kinetic energy (TKE), $k_{t(nb)}$, estimated from the predicted $\langle U \rangle_d$ (Equation 22) and U_{nb} (Equation 7). (c) Deposition distribution, $Dep/Dep_{(p=1)}$, estimated from two predicted near-bed turbulent kinetic energy in subplot (b). In each subplot, solid lines represent predictions, and dashed lines are their uncertainties. The measured depth-averaged velocity and near-bed velocity in subplot (a) and measured deposition in subplot (c) are from Case 4 ($H = 20$ cm, $U_0 = 17$ cm/s, $\phi = 0.015$).

In the fully developed flow region:

$$\langle U_{(f)} \rangle_d = \sqrt{\frac{2gS(1-\phi)}{C_d a_d}} \tag{21}$$

The depth-averaged velocity can be used in Equation 7 to predict near-bed TKE

$$k_{t(nb)} = \frac{C_f}{\omega} \langle U \rangle_d^2 + \gamma^2 \left(C_d \frac{n d_{ms}^2}{2(1-\phi)} \right)^{2/3} \langle U \rangle_d^2 \tag{22}$$

As an example, consider Case 4 (Figure 10, $H = 20$ cm, $U_0 = 17$ cm/s, $\phi = 0.015$). The predicted depth-averaged velocity (Equation 20, black line in Figure 10a) had good agreement with the measured depth-average velocity (circles), but was smaller than the measured near-bed velocity (red diamonds). This was expected, since the frontal area ($a_{nb} = 0.02\, cm^{-1}$, Equation 5) in the near-bed region was smaller than the depth-averaged frontal area ($a_d = 0.062\, cm^{-1}$, Equation 21). However, the difference in velocity was sufficiently small that the near-bed TKE predicted from the near-bed velocity (Equation 7) and from the depth-averaged velocity (Equation 22) were the same within uncertainty (Figure 10b) and thus produced the same distribution of deposition (Figure 10c). The comparison indicated that for some canopies, the depth-averaged velocity could provide a reliable prediction of near-bed TKE and deposition.

5.4. Model Limitation

The proposed model was shown to give good predictions for deposition inside emergent canopies of *P. australis* with real morphology and with solid volume fraction $\phi \leq 0.02$. Because the model assumes the suspended

concentration is the same inside and outside of the canopy, it cannot reflect conditions with supply limitation, which occurs if the transport time-scale through the canopy, $L/\langle U_{(f)}$, is comparable to the settling time-scale, H/w_s (e.g., see discussion in Zong & Nepf, 2010). Specifically, for $L/\langle U_{(f)}\rangle \geq H/w_{s,}$ the progressive deposition of particles along the canopy length is sufficient to diminish the suspended concentration, such that the supply of suspended sediment available for deposition decreases along the canopy length. The proposed model will be accurate if $L/\langle U_{(f)}\rangle << H/w_s$, and one should confirm these conditions before applying the model. Based on these time-scales, the tendency for supply limitation increases with increasing canopy length and increasing canopy density (associated with decreasing canopy velocity). In addition, the model assumes that vegetation-generated turbulence is present, which requires that the stem Reynolds number, Re_d, be larger than 120 (Liu & Nepf, 2016).

6. Conclusions

A finite canopy of *P. australis* was constructed along the sidewall of an open channel. Near-bed velocity, TKE, and sediment deposition were measured within the canopy at different longitudinal positions. Models to predict velocity, TKE, and deposition along the canopy were discussed and validated. Relative to an upstream reference, the net deposition within the canopy was enhanced when two conditions were met: the local near-bed TKE was smaller than the critical value for resuspension, and resuspension took place in the bare channel. Because vegetation-generated turbulence impacts resuspension, a new model using near-bed TKE provided a better prediction of deposition than models based on bed-shear stress. The proposed model provided a way to estimate the critical solid volume fraction, ϕ_c, above which deposition inside a canopy would be enhanced relative to deposition in adjacent bare beds. When resuspension occurred in the bare channel, ϕ_c was shown to be independent of channel-average velocity and sediment size, but decreased as the canopy length increased. Assuming the same solid volume fraction, plant morphology did not have a strong impact on deposition within the canopy.

Data Availability Statement

All data presented in the paper are available through Figshare at this site (https://doi.org/10.6084/m9.figshare.20337672.v1).

Acknowledgments
This study received financial support from the Sichuan Science and Technology Program (2021YFH0028 and 2022NSFSC0969), the National Natural Science Foundation of China (52022063 and 52179074) and the Fok Ying Tung Education Foundation (171067). We acknowledge Fujian Li for helping us process plant images and Qi Wang for helping us setup experiments.

References

Belcher, S. E., Jerram, N., & Hunt, J. C. R. (2003). Adjustment of a turbulent boundary layer to a canopy of roughness elements. *Journal of Fluid Mechanics*, *488*, 369–398. https://doi.org/10.1017/S0022112003005019

Bellavance, M. E., & Brisson, J. (2010). Spatial dynamics and morphological plasticity of common reed (Phragmites australis) and cattails (Typha sp.) in freshwater marshes and roadside ditches. *Aquatic Botany*, *93*(2), 129–134. https://doi.org/10.1016/j.aquabot.2010.04.003

Biron, P. M., Robson, C., Lapointe, M. F., & Gaskin, S. J. (2004). Comparing different methods of bed shear stress estimates in simple and complex flow fields. *Earth Surface Processes and Landforms: The Journal of the British Geomorphological Research Group*, *29*(11), 1403–1415. https://doi.org/10.1002/esp.1111

Bouma, T. J., Duren, L. A. V., Temmerman, S., Claverie, T., Blanco-Garcia, A., Ysebaert, T., & Herman, P. M. J. (2007). Spatial flow and sedimentation patterns within patches of epibenthic structures: Combining field, flume and modeling experiments. *Continental Shelf Research*, *27*(8), 1020–1045. https://doi.org/10.1016/j.csr.2005.12.019

Caroppi, G., Gualtieri, P., Fontana, N., & Giugni, M. (2020). Effects of vegetation density on shear layer in partly vegetated channels. *Journal of Hydro-Environment Research*, *30*, 82–90. https://doi.org/10.1016/j.jher.2020.01.008

Chen, Z., Jiang, C., & Nepf, H. (2013). Flow adjustment at the leading edge of a submerged aquatic canopy. *Water Resources Research*, *49*(9), 5537–5551. https://doi.org/10.1002/wrcr.20403

Cheng, N. S. (1997). Effect of concentration on settling velocity of sediment particles. https://doi.org/10.1061/(ASCE)0733-9429(1997)123:8(728)

Cornacchia, L., Van De Koppel, J., Van Der Wal, D., Wharton, G., Puijalon, S., & Bouma, T. J. (2018). Landscapes of facilitation: How self-organized patchiness of aquatic macrophytes promotes diversity in streams. *Ecology*, *99*(4), 832–847. https://doi.org/10.1002/ecy.2177

Cotton, J., Wharton, G., Bass, J., Heppell, C., & Wotton, R. (2006). The effects of seasonal changes to in-stream vegetation cover on patterns of flow and accumulation of sediment. *Geomorphology*, *77*(3–4), 320–334. https://doi.org/10.1016/j.geomorph.2006.01.010

Elliott, S. H., Tullos, D. D., & Walter, C. (2019). Physical modeling of the feedbacks between a patch of flexible Reed Canarygrass (*Phalaris arundinacea*), wake hydraulics, and downstream deposition. *Environmental Fluid Mechanics*, *19*(1), 255–277. https://doi.org/10.1007/s10652-018-9622-8

Engelund, F., & Fredsoe, J. (1976). A sediment transport model for straight alluvial channels. *Hydrology Research*, *7*(5), 293–306. https://doi.org/10.2166/nh.1976.0019

Etminan, V., Ghisalberti, M., & Lowe, R. J. (2018). Predicting bed shear stresses in vegetated channels. *Water Resources Research*, *54*(11), 9187–9206. https://doi.org/10.1029/2018WR022811

Etminan, V., Lowe, R. J., & Ghisalberti, M. (2017). A new model for predicting the drag exerted by vegetation canopies. *Water Resources Research*, *53*(4), 3179–3196. https://doi.org/10.1002/2016WR020090

Gacia, E., Soto, D. X., Roig, R., & Catalan, J. (2021). *Phragmites australis* as a dual indicator (air and sediment) of trace metal pollution in wetlands–the key case of Flix reservoir (Ebro River). *Science of the Total Environment*, *765*, 142789. https://doi.org/10.1016/j.scitotenv.2020.142789

Goring, D. G., & Nikora, V. I. (2002). Despiking acoustic Doppler velocimeter data. *Journal of Hydraulic Engineering*, *128*(1), 117–126. https://doi.org/10.1061/(ASCE)0733-9429(2002)128:1(117)
Gu, J., Shan, Y., Liu, C., & Liu, X. (2019). Feedbacks of flow and bed morphology from a submerged dense vegetation patch without upstream sediment supply. *Environmental Fluid Mechanics*, *19*(2), 475–493. https://doi.org/10.1007/s10652-018-9633-5
Hauber, D. P., Saltonstall, K., White, D. A., & Hood, C. S. (2011). Genetic variation in the common reed, *Phragmites australis*, in the Mississippi river delta marshes: Evidence for multiple introductions. *Estuaries and Coasts*, *34*(4), 851–862. https://doi.org/10.1007/s12237-011-9391-9
Huai, W. X., Li, S., Katul, G. G., Liu, M. Y., & Yang, Z. H. (2021). Flow dynamics and sediment transport in vegetated rivers: A review. *Journal of Hydrodynamics*, *33*(3), 400–420. https://doi.org/10.1007/s42241-021-0043-7
Huai, W. X., Zhang, J., Wang, W. J., & Katul, G. G. (2019). Turbulence structure in open channel flow with partially covered artificial emergent vegetation. *Journal of Hydrology*, *573*, 180–193. https://doi.org/10.1016/j.jhydrol.2019.03.071
Julien, P. Y. (2010). *Erosion and sedimentation*. Cambridge University Press.
Kim, H. S., Kimura, I., & Park, M. (2018). Numerical simulation of flow and suspended sediment deposition within and around a circular patch of vegetation on a rigid bed. *Water Resources Research*, *54*(10), 7231–7251. https://doi.org/10.1029/2017WR021087
Kim, H. S., Kimura, I., & Shimizu, Y. (2015). Bed morphological changes around a finite patch of vegetation. *Earth Surface Processes and Landforms*, *40*(3), 375–388. https://doi.org/10.1002/esp.3639
Licci, S., Nepf, H., Delolme, C., Marmonier, P., Bouma, T., & Puijalon, S. (2019). The role of patch size in ecosystem engineering capacity: A case study of aquatic vegetation. *Aquatic Sciences*, *81*(3), 41. https://doi.org/10.1007/s00027-019-0635-2
Lightbody, A. F., & Nepf, H. M. (2006). Prediction of velocity profiles and longitudinal dispersion in salt marsh vegetation. *Limnology & Oceanography*, *51*(1), 218–228. https://doi.org/10.4319/lo.2006.51.1.0218
Li, F., Shan, Y., Huang, S., Liu, C., & Liu, X. (2021). Flow depth, velocity, and sediment motions in a straight widened channel with vegetated floodplains. *Environmental Fluid Mechanics*, *21*(2), 483–501. https://doi.org/10.1007/s10652-021-09783-9
Liu, C., & Nepf, H. (2016). Sediment deposition within and around a finite patch of model vegetation over a range of channel velocity. *Water Resources Research*, *52*(1), 600–612. https://doi.org/10.1002/2015WR018249
Liu, C., & Shan, Y. (2019). Analytical model for predicting the longitudinal profiles of velocities in a channel with a model vegetation patch. *Journal of Hydrology*, *576*, 561–574. https://doi.org/10.1016/j.jhydrol.2019.06.076
Liu, C., & Shan, Y. (2022). Impact of an emergent model vegetation patch on flow adjustment and velocity. *Proceedings of the Institution of Civil Engineers-Water Management*, *175*(2), 55–66. https://doi.org/10.1680/jwama.20.00108
Liu, C., Shan, Y., Liu, X., Yang, K., & Liao, H. (2016). The effect of floodplain grass on the flow characteristics of meandering compound channels. *Journal of Hydrology*, *542*, 1–17. https://doi.org/10.1016/j.jhydrol.2016.07.037
Liu, C., Shan, Y., & Nepf, H. (2021). Impact of stem size on turbulence and sediment resuspension under unidirectional flow. *Water Resources Research*, *57*(3), e2020WR028620. https://doi.org/10.1029/2020WR028620
Liu, C., Shan, Y., Sun, W., Yan, C., & Yang, K. (2020). An open channel with an emergent vegetation patch: Predicting the longitudinal profiles of velocities based on exponential decay. *Journal of Hydrology*, *582*, 124429. https://doi.org/10.1016/j.jhydrol.2019.124429
Losada, I. J., Maza, M., & Lara, J. L. (2016). A new formulation for vegetation-induced damping under combined waves and currents. *Coastal Engineering*, *107*, 1–13. https://doi.org/10.1016/j.coastaleng.2015.09.011
Manners, R. B., Wilcox, A. C., Li, K., Lightbody, A. F., Stella, J. C., & Sklar, L. S. (2015). When do plants modify fluvial processes? Plant-hydraulic interactions under variable flow and sediment supply rates. *Journal of Geophysical Research: Earth Surface*, *120*(2), 325–345. https://doi.org/10.1002/2014JF003265
Nepf, H. (2012). Flow and transport in regions with aquatic vegetation. *Annual Review of Fluid Mechanics*, *44*(1), 123–142. https://doi.org/10.1146/annurev-fluid-120710-101048
O'Hare, M. T., McGahey, C., Bissett, N., Cailes, C., Henville, P., & Scarlett, P. (2010). Variability in roughness measurements for vegetated rivers near base flow. *England and Scotland*, *385*(1–4), 361–370. https://doi.org/10.1016/j.jhydrol.2010.02.036
Ortiz, A. C., Ashton, A., & Nepf, H. M. (2013). Mean and turbulent velocity fields near rigid and flexible plants and the implications for deposition. *Journal of Geophysical Research: Earth Surface*, *118*(4), 2585–2599. https://doi.org/10.1002/2013jf002858
Rominger, J. T., & Nepf, H. (2011). Flow adjustment and interior flow associated with a rectangular porous obstruction. *Journal of Fluid Mechanics*, *680*, 636–659. https://doi.org/10.1017/jfm.2011.199
Sand-Jensen, K. A. J., & Pedersen, M. L. (2008). Streamlining of plant patches in streams. *Freshwater Biology*, *53*(4), 714–726. https://doi.org/10.1111/j.1365-2427.2007.01928.x
Shan, Y., Liu, C., & Nepf, H. (2019). Comparison of drag and velocity in model mangrove forests with random and in-line tree distributions. *Journal of Hydrology*, *568*, 735–746. https://doi.org/10.1016/j.jhydrol.2018.10.077
Shan, Y., Liu, X., Yang, K., & Liu, C. (2017). Analytical model for stage-discharge estimation in meandering compound channels with submerged flexible vegetation. *Advances in Water Resources*, *108*, 170–183. https://doi.org/10.1016/j.advwatres.2017.07.021
Shan, Y., Zhao, T., Liu, C., & Nepf, H. (2020). Turbulence and bed-load transport in channels with randomly distributed emergent patches of model vegetation. *Geophysical Research Letters*, *47*(12), 143–153. https://doi.org/10.1029/2020GL087055
Shi, Y., Jiang, B., & Nepf, H. (2016). Influence of particle size and density, and channel velocity on the deposition patterns around a circular patch of model vegetation. *Water Resources Research*, *52*(2), 1044–1055. https://doi.org/10.1002/2015WR018278
Soulsby, R. (1981). Measurement of the Reynolds stress components close to a marine sand bank. *Marine Geology*, *42*(1–4), 35–47. https://doi.org/10.1016/0025-3227(81)90157-2
Tanino, Y., & Nepf, H. (2008). Lateral dispersion in random cylinder arrays at high Reynolds number. *Journal of Fluid Mechanics*, *600*, 339–371. https://doi.org/10.1017/S0022112008000505
Tinoco, R. O., & Coco, G. (2016). A laboratory study on sediment resuspension within arrays of rigid cylinders. *Advances in Water Resources*, *92*, 1–9. https://doi.org/10.1016/j.advwatres.2016.04.003
Toth, V. R., & Szabo, K. (2012). Morphometric structural analysis of *Phragmites australis* stands in Lake Balaton. *Annales de Limnologie - International Journal of Limnology*, *48*(2), 241–251. https://doi.org/10.1051/limn/2012015
Tseng, C. Y., & Tinoco, R. O. (2021). A two layer turbulence based model to predict suspended sediment concentration in flows with aquatic vegetation. *Geophysical Research Letters*, *48*(3), e2020GL091255. https://doi.org/10.1029/2020GL091255
Vandenbruwaene, W., Temmerman, S., Bouma, T. J., Klaassen, P. C., de Vries, M. B., Callaghan, D. P., et al. (2011). Flow interaction with dynamic vegetation patches: Implications for biogeomorphic evolution of a tidal landscape. *Journal of Geophysical Research*, *116*(F1), 155–170. https://doi.org/10.1029/2010jf001788
White, B., & Nepf, H. (2007). Shear instability and coherent structures in a flow adjacent to a porous layer. *Journal of Fluid Mechanics*, *593*, 1–32. https://doi.org/10.1017/S0022112007008415

White, B. L., & Nepf, H. (2008). A vortex-based model of velocity and shear stress in a partially vegetated shallow channel. *Water Resources Research*, *44*(1), W01412. https://doi.org/10.1029/2006WR005651

White, F. M. (1991). *Viscous fluid flow [M]* (2nd ed.). McGraw-Hill.

Widdows, J., Pope, N. D., & Brinsley, M. D. (2008). Effect of *Spartina anglica* stems on near-bed hydrodynamics, sediment erodability and morphological changes on an intertidal mudflat. *Marine Ecology Progress Series*, *362*, 45–57. https://doi.org/10.3354/meps07448

Xu, Y., & Nepf, H. (2020). Measured and predicted turbulent kinetic energy in flow through emergent vegetation with real plant morphology. *Water Resources Research*, *56*(12), e2020WR027892. https://doi.org/10.1029/2020WR027892

Yager, E., & Schmeeckle, M. (2013). The influence of vegetation on turbulence and bed load transport. *Journal of Geophysical Research: Earth Surface*, *118*(3), 1585–1601. https://doi.org/10.1002/jgrf.20085

Yang, J. Q., Chung, H., & Nepf, H. (2016). The onset of sediment transport in vegetated channels predicted by turbulent kinetic energy. *Geophysical Research Letters*, *43*(21), 11–261. https://doi.org/10.1002/2016GL071092

Yang, J. Q., Kerger, F., & Nepf, H. M. (2015). Estimation of the bed shear stress in vegetated and bare channels with smooth beds. *Water Resources Research*, *51*(5), 3647–3663. https://doi.org/10.1002/2014WR016042

Yang, J. Q., & Nepf, H. M. (2019). Impact of vegetation on bed load transport rate and bedform characteristics. *Water Resources Research*, *55*(7), 6109–6124. https://doi.org/10.1029/2018WR024404

Zhang, J., Lei, J., Huia, W., & Nepf, H. (2020). Turbulence and particle deposition under steady flow along a submerged seagrass meadow. *Journal of Geophysical Research: Oceans*, *125*(5), e2019JC015985. https://doi.org/10.1029/2019JC015985

Zhao, T., & Nepf, H. M. (2021). Turbulence dictates bedload transport in vegetated channels without dependence on stem diameter and arrangement. *Geophysical Research Letters*, *48*(21), e2021GL095316. https://doi.org/10.1029/2021GL095316

Zong, L., & Nepf, H. (2010). Flow and deposition in and around a finite patch of vegetation. *Geomorphology*, *116*(3–4), 363–372. https://doi.org/10.1016/j.geomorph.2009.11.020

Zong, L., & Nepf, H. (2011). Spatial distribution of deposition within a patch of vegetation. *Water Resources Research*, *47*(3), W03516. https://doi.org/10.1029/2010WR00951